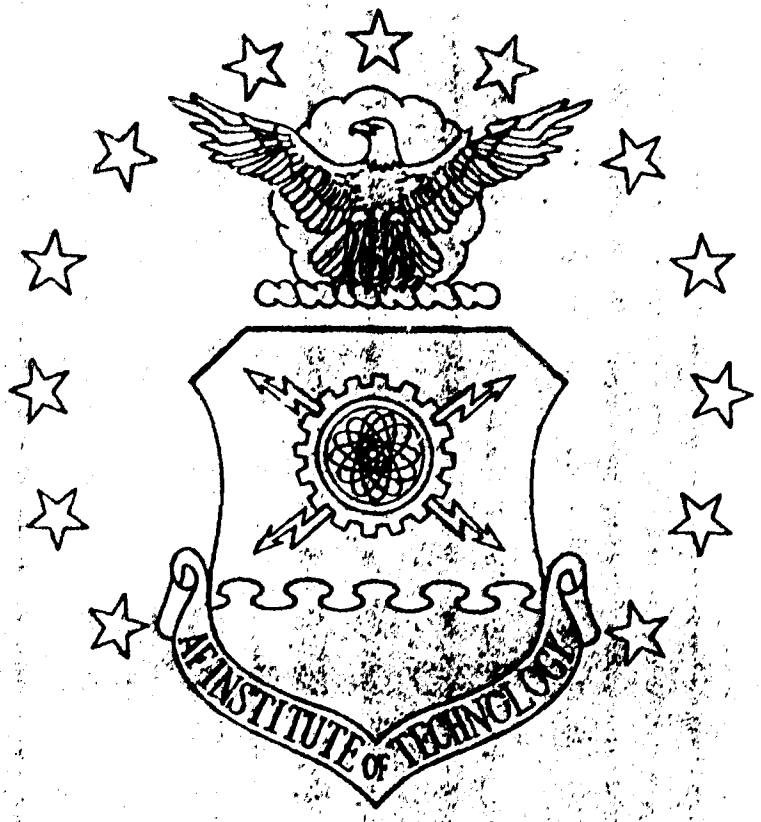

EFFECT OF RIBLETS ON PRESSURE RECOVERY IN A STRAIGHT-WALLED DIFFUSER

THESIS

Michael K. Reagan
Captain, USAF

AFIT/GAE/ENY/90D-21

DEPARTMENT OF THE AIR FORCE
AIR UNIVERSITY
AIR FORCE INSTITUTE OF TECHNOLOGY

Wright-Patterson Air Force Base, Ohio

AFIT/GAE/ENY/90D-21

EFFECT OF RIBLETS ON PRESSURE RECOVERY IN A STRAIGHT-WALLED DIFFUSER

THESIS

Michael K. Reagan
Captain, USAF

AFIT/GAE/ENY/90D-21

AFIT/GAE/ENY/90D-21

EFFECT OF RIBLETS ON PRESSURE RECOVERY IN A STRAIGHT-WALLED DIFFUSER

THESIS

Presented to the Faculty of the School of Engineering
of the Air Force Institute of Technology
Air University
In Partial Fulfillment of the
Requirements for the Degree of
Master of Science in Aeronautical Engineering

Michael K. Reagan, B.S.
Captain, USAF

December 1990

Approved for public release; distribution unlimited

Preface

The undertaking of an experimental thesis entails with it a lot of frustration and hopefully, some interesting results. Having never done anything like this before, I was filled with a great deal of anticipation and a wee bit of trepidation. The former got me through many nights in the lab and the later kept me up the other nights.

Fortunately, I was guided through this investigation by the best of them. My personal thanks to Lt Col, now retired, Paul King, Dr William Elrod and Dr Milton Franke for their patience and understanding during the stay of this work. Their insight and many years of experience helped make this experiment a very enjoyable and thought-provoking one.

Thanks must also go to the AFIT Model Shop; specifically, Mr Jack Tiffany and Mr Dave Driscoll. Their outstanding support and advice on model design and construction was invaluable in the successful completion of this work.

I owe a debt of gratitude to the laboratory supervisor, Mr Nick Yardich and his superb team; specifically, Mr Dan Rioux and Mr Jay Anderson, for a job well done in providing top-notch support. As with most experiments, equipment problems seem to plague the research effort. Thanks to these fine gentlemen, I had no such problems--bravo!

Finally, to Ms Kate Schultz, for always have a friendly smile and a cheerful hello--ODIWMY.

Table of Contents

List of Figures

List of Tables

List of Symbols

Symbols		Units
A,B,C,D,E	hot-film anemometer constants	none
A,B,C	multiplicative parameters in Stratford's criteria	none
A_x	diffuser area at location x measured along the ramp	ft^2
c	Cole's integration constant (range 4.9 to 5.5)	none
C_f	skin friction coefficient	none
C_p	pressure coefficient	none
$C_{p\,ideal}$	ideal pressure coefficient	none
dC_p/dx	pressure distribution	none
dp/dy	pressure distribution through boundary layer normal to surface	lbf/ft^3
du/dy	velocity distribution through the boundary layer	sec^{-1}
D_h	hydraulic diameter	ft
E_b	bridge output voltage	volts
$F(x)$	Stratford's criteria separation parameter	none
g	local acceleration constant	ft/sec^2
h	riblet peak-to-valley height	ft
h^+	nondimensional riblet peak-to-valley height	none
H	one-half of diffuser throat width	ft
L	length of diffuser ramp measured from throat	ft
L/W	diffuser aspect ratio	none
P_x	static pressure at location x	lbf/ft^2
P_{static}	static pressure	lbf/ft^2
P_{sw}	tunnel sidewall pressure	lbf/ft^2

P_T	total pressure	lbf/ft^2
P_{atm}	atmospheric pressure	lbf/ft^2
q	dynamic pressure	lbf/ft^2
R	air gas constant	Btu/lbm $^\circ$R
Re_x	Reynolds number, $Re_x=U_e x/\nu$	none
Re_d	Reynolds number, $Re_d=U_e D_h/\nu$	none
s	riblet peak-to-peak width	ft
s^+	nondimensional riblet peak-to-peak width	none
T	temperature	F
U	freestream velocity	ft/sec
U_e	boundary layer edge velocity	ft/sec
U_o	velocity at beginning of adverse presure gradient	ft/sec
U_{th}	diffuser throat velocity	ft/sec
U_τ	friction velocity	ft/sec
u+	dimensionless velocity parameter	none
W	diffuser width at throat, W=2H	ft
$w(y/\delta)$	Cole's wake function	none
x	distance measure along diffuser surface from divergence point	ft
x_{sep}	location of separation measured from minimum pressure point	ft
x/L	nondimensional ramp distance	none
Δx_{sep}	change in separation location	ft
y	distance measured normal to diffuser surface	ft
y^+	nondimensional distance normal to ramp surface	none

δ	boundary layer thickness measured normal to surface	ft
ϵ	error parameter	none
ϵ_{rms}	root-mean-square error value	none
η	Blasius solution flow constant	none
η_d	diffuser efficiency	none
θ	one-half of included diffuser divergence angle	deg
2θ	included diffuser divergence angle	deg
κ	von Karman's mixing length constant	none
ν	kinematic viscosity	ft^2/sec
$\Pi(x)$	Cole's profile parameter	none
ρ	fluid density	lbm/ft^3
$\phi_1(y^+)$	turbulent boundary layer law-of-the-wall function	none

Abstract

The objective of this thesis was to investigate the effect of riblets on the pressure recovery in a straight-walled diffuser. Previous work has shown that riblets were effective in reducing the viscous drag over surfaces subjected to a turbulent boundary layer. More recently, riblets were shown to delay the flow separation within a subsonic, straight-walled diffuser by as much as 200 percent. The purpose of this investigation was to determine the effect on the pressure distribution within a diffuser that has had the flow separation point favorably altered by the application of riblets.

Results from this investigation revealed that riblets not only delayed flow separation in a diffuser, but also altered the pressure distribution in a manner that allowed for improved pressure recovery. This improvement was realized by an increase in the pressure coefficient of between 30 and 38 percent, the larger increases occurring for those diffuser geometries most likely leading to stall (high aspect ratio). Additionally, it was discovered that the introduction of static ports into the riblet surface did not significantly alter the flowfield over that of a geometrically similar riblet surface.

EFFECT OF RIBLETS ON PRESSURE RECOVERY IN A STRAIGHT-WALLED DIFFUSER

I. Introduction

The primary purpose of this thesis was to experimentally investigate the effect of riblets on the pressure recovery in a straight-walled, subsonic diffuser. Riblets are small flow-aligned grooves that were originally introduced in 1979 as a passive means for reducing viscous drag over a body subjected to turbulent flow (20:168). Later experiments showed that flow separation was delayed in a straight-walled diffuser by as much as 200 percent (17:58). However, no work has been done to determine the effect of riblets on the pressure distribution within diffusers. Specifically, what happens to the pressure recovery in a diffuser with riblets that has been experimentally shown to delay flow separation? This thesis employed a geometrically similar diffuser shape to the one used previously by Martens (17:22) in his investigation of flow separation due to riblets. The research effort attempted to first duplicate the results obtained by Martens and then obtain surface pressure distributions for both a smooth and riblet diffuser surface to determine the effect on diffuser pressure recovery.

Background

Riblets were originally introduced in 1979 as a means of reducing the viscous drag over hydrodynamic surfaces subjected to turbulent boundary layers. Their application to aerodynamic surfaces (i.e., cylinders, airfoils and diffusers) for the same purpose has been investigated with vigor over the years, especially at the Air Force Institute of Technology (AFIT). Results of these investigations have shown that riblets delay the occurrence of flow separation in subsonic diffusers as well as cylinders and airfoils, with the most dramatic change occurring in the diffuser.

In the work done by Wieck (22:55,56), a change in the surface pressure distribution was evident with the application of riblets to both the cylinder and airfoil shapes. No work was done to quantify this change in surface pressure but a recommendation was made to do so with the diffuser model used in experiments by Martens in 1988. The reason for this was due to the fact that significant delays in flow separation were obtained for the diffuser whereas only minor, but noticeable, delays were noticed for the airfoil and cylinder and any small changes in the pressure distribution would be more visible with the diffuser.

Given this impetus, it was decided to investigate the effect of riblets on the surface pressure distribution using an identical model to that used in the Martens work. This allowed a comparison of separation data to that obtained previously, thus lending more credence to the data collection techniques. The surface pressure distributions were obtained using static ports built into the diffuser ramp. Because of the low subsonic speeds involved, hot-wire anemometry and a Pitot tube were

utilized to verify these pressure measurements. Comparisons of the pressure distributions before and after riblet application provided the necessary insight from which to draw conclusions.

Objective

The primary objective of this research was to investigate the effect of riblets on the pressure recovery in a straight-walled subsonic diffuser. The scope of the work involved determining changes in the flow separation points by the addition of riblets for varying diffuser geometries and throat velocities and comparing these changes to changes in the surface pressure distribution.

II. Theory

Riblets

Since their introduction more than ten years ago, riblets have been used primarily as a quick, convenient method of reducing viscous drag on aerodynamic and hydrodynamic bodies. Extensive experimental work has shown that the viscous drag associated with these shapes was reduced by as much as eight percent (21:1,4). This reduction in drag was primarily attributed to the ability of riblets to control and damp turbulence, thereby reducing turbulent shear. The caveat to these experiments was of course, the existence of a turbulent boundary layer and a short discussion on this seems appropriate.

Every known fluid offers a resistance to the relative sliding motion of any two adjacent layers. This property, viscosity, is noticeable only when the fluid is in motion (7:9,10). For fluids of relatively small viscosity, the effects are concentrated in a thin layer surrounding the body called a boundary layer (11:40; 16:299). Within this layer, the flow can be classified as laminar, turbulent or in a state of transition between the two states (3:170). Figure 1 shows the relative location of these three flow regimes along a flat plate.

Laminar flow occurs at low Reynolds number and is characterized by a relatively thin layer with limited momentum transfer and eddy motion. The turbulent boundary layer on the other hand, is considerably thicker than a laminar layer and is characterized by the presence of a relatively large number of eddies. These eddies serve as a type of momentum transfer vehicle between the fast moving flow at the outer

edge of the boundary layer and the slow moving fluid closer to the surface. This results in a higher velocity gradient near the surface and a proportionately higher value of skin friction.

The turbulent boundary layer is usually treated as a composite layer consisting of inner and outer regions. The inner region is only 10-20 percent of the entire boundary layer thickness and is further divided in the viscous (or laminar) sublayer, the transitional region (buffer layer), and the fully turbulent region (5:94). Figure 2 shows the relationship between these three regions for the case of no pressure gradient.

The viscous drag reduction capability of riblets appears to be related to their ability to control and damp the "hairpin-like" vortices associated with the turbulent eddies. The interaction of riblets with the counter-rotating streamwise turbulent vortices results in the generation of a secondary vortex which begins at the riblet peak and extends down into the riblet valley as shown in Figure 3 (2:1384). As these secondary vortices are generated, the primary streamwise vortices are weakened, and the mechanism by which momentum is transferred within the boundary layer is made less effective. This tends to retard the development of the turbulent boundary layer on the riblet surface. Anders describes this as the generation of, ". . .a relatively quiescent flow in the riblet valley that pushes skin-friction producing turbulence up and away from the surface" (1:26).

The most important parameter in the ability of riblets to reduce viscous drag is their size. Extensive testing has shown that in order for riblets to be effective, they must extend through the viscous sublayer and into the transitional region of the boundary layer. The two

nondimensional parameters affecting riblet performance are the peak-to-valley height (h^+) and the peak-to-peak width (s^+) defined as follows (19:1):

$$h^+ = hU_\tau/\nu \tag{1}$$

$$s^+ = sU_\tau/\nu \tag{2}$$

A number of studies have shown that the maximum drag reduction for V-grooved shaped riblets applied to a flat plate occurred for h^+ values between 8 and 15. Furthermore, riblets continued to show the ability to reduce drag for values of h^+ up tp 30. (20:168). From Eq (1), the optimal riblet size for use in the diffuser can be determined using the following relationship:

$$y = y^+\nu/U_\tau \tag{3}$$

The optimal riblet size corresponds to setting y^+ to a value between 10 and 30 (the transitional region) in Eq (3). Since the kinematic viscosity is basically a constant for air over a fairly wide range of temperatures, the only parameter that needs to be estimated is U_τ, the friction velocity. This is defined as:

$$U_\tau = U_e(C_f/2)^{0.5} \tag{4}$$

C_f can be estimated by the following empirical relationship for turbulent flow over a flat plate (16:401):

$$C_f = 0.0592(Re_x)^{(-.2)} \quad (5)$$

and U_e is defined as the boundary layer edge velocity. The range of velocities used in the wind tunnel ranged from static conditions to approximately 65 ft/sec. Using the above equations, an estimate of the optimal riblet height for use in the diffuser section can be made. In the previous experiment, the ideal riblet height for the flow velocities investigated was found to be Ø.Ø35 in.

Flow Separation

Because viscosity is present in real world flows, there is a natural tendency for adjacent layers of the flow to retard one another. The velocity of the fluid at the surface must be zero and steadily increase throughout the boundary layer until it approaches the freestream value. All of the losses associated with viscosity are contained within this boundary layer. The flow around any aerodynamic body will always generate a boundary layer. The extent to which the flow separates is dependant on the rate of growth of the boundary layer. In fact, the rate of growth, ". . .may be so rapid that the fluid is unable to flow along the surface, and breaks away instead of following the body outline" (3:187). The particular point where the flow breaks away is defined as the separation point.

Separation can occur only in an adverse pressure gradient. An adverse pressure gradient is defined as one for which the pressure is increasing in the direction of flow. Given that an incoming flow has a certain amount of energy, as the flow continues around an aerodynamic

surface, a boundary layer is formed. Due to the viscous forces present in the boundary layer, a portion of the energy in the boundary layer profile is converted from directed kinetic energy into heat energy of some other form. This results in a deviation to the velocity profile as seen in Figure 4 (8:68). At the point on the surface where the slope of the velocity profile, (dU/dy), goes to zero, there is no flow present and separation has occurred. In fact, ". . .separation of the boundary results from the presence of the adverse pressure gradient" (16:315). Figure 4 suggests that there is a recirculating region beyond the separation point. In practice, this is a highly unstable region and the flow may or may not exist there in a recirculating mode (8:68).

Therefore, two necessary and sufficient conditions for flow separation are viscosity (which is always present) and the existence of an adverse pressure gradient. Due to the highly diffusive nature of turbulent boundary layers, they are able to resist flow separation much better than a laminar layer. In applications, it is sometimes preferable to have turbulent flow rather than laminar. One must always consider however, the tradeoff with the increase in viscous drag associated with turbulent layers.

Numerical methods exist and provide good estimates for predicting flow separation in turbulent boundary layers. The method employed for this thesis was Stratford's criteria. The same method was used in the 1988 study by Martens and results from that experiment showed good correlation between the predicted and actual separation points. This author found no need to change a procedure that had been shown to work.

The Stratford method consists of using the following equation as a predictor in flow separation (5:2Ø4):

$$F(x) = C_p(x dC_p/dx)^{0.5}(10^{(-6)}R_x)^{(-.1)} \quad (6)$$

Eq (6) ". . . assumes an adverse pressure gradient starting from the leading edge, as well as fully turbulent flow everywhere" (5:2Ø4). In the case of the diffuser, the equation assumes the adverse pressure gradient forms at the beginning of the diverging ramp. This equation was modified in a similar manner to the Martens work and the result presented as Eq (7) below. The derivation of Eq (7) may be found at Appendix A:

$$F(x) = (A)(B)(C) \quad (7)$$

where: $A = [1-H^2/(H+x\sin\theta)^2]$

$B = [2xH^2\sin\theta/(H+x\sin\theta)^3]^{0.5}$

$C = (Re_x 10^{-6})^{-1}$

and: H = diffuser throat height (ft)

θ = ramp divergence angle (deg)

Eq (7) was used to predict the flow separation in the diffuser over the range of geometries and velocities. "For a typical turbulent boundary layer with an adverse pressure gradient, it is found that F(x) increases as separation is approached and decreases after separation." Stratford used a specific range on F(x) to determine the separation point. By

comparison with experiment he noted that, ". . .if the maximum value of F(x) is (a) greater than Ø.4Ø, separation is predicted when F(x) = Ø.4Ø; (b) between Ø.35 and Ø.4Ø, separation occurs at the maximum value; (c) less than Ø.35, separation does not occur" (5:2Ø5). This same criteria was used in this investigation.

Diffuser

A diffuser is a device used in engineering applications to decelerate fluid flow. Perhaps the most well-known use of diffusers is in aircraft engines. For example, in a typical turbojet or turbofan, a diffuser is used to decelerate the incoming flow to an acceptable velocity for the compressor. Additional uses are found at the exit of the compressor and turbines in order to slow the flow prior to combustion in the main burner and augmentor (18:3Ø5).

Physically, a subsonic diffuser is nothing more than a device with diverging walls. It may be rectangular, square, circular or conical. Its primary function is to convert kinetic energy into pressure energy. Diffuser performance is a measure of how well it performs its primary function. There are a number of ways to measure a diffuser's performance. The method used in this investigation dealt with diffuser efficiency defined as (18:3Ø6):

$$\eta_d = C_p / C_{p_{ideal}} \tag{8}$$

where: C_p = pressure coefficient

$C_{p_{ideal}}$ = ideal pressure coefficient

The actual pressure coefficient is defined as the ratio of the difference in static pressures between stations 1 and 2 in a diffuser to the dynamic pressure at station 1:

$$C_p = (P_2 - P_1)/\{0.5\rho U_1^2\} \tag{9}$$

Using continuity, the ideal pressure coefficient at station 2 can be shown to be:

$$C_{p\,ideal} = 1 - (A_1/A_2)^2 \tag{10}$$

where A refers to the cross-sectional area of the diffuser at any location. If station 1 is taken as the throat condition, then the pressure coefficient at the throat will equal zero and all subsequent coefficients will increase. The amount of increase in the pressure coefficient from the throat value of zero is termed the pressure recovery.

Two primary parameters used in describing the flow behavior in diffusers are the aspect ratio, (L/W) and the divergence angle, (2θ). When the design of these two parameters is optimized, the flow is well-behaved with minimum losses. However, deviations from the optimum conditions result in a dramatic increase in losses due to separation (15:327). Figure 5 shows a plot of diffuser geometry and separation regimes for straight-walled diffusers. This data was generated from extensive testing done in the late 1950's by Kline (14:307), and provides a guide for the optimum design of diffusers. The line on Figure 5 that separates the area of no stall from that of appreciable stall is of particular interest. Design in the area of appreciable stall is to be avoided

since the static pressure recovery decreases, mixing losses increase and areas of severe flow asymmetry and unsteadiness result--all of which are detrimental to the efficient operation of a diffuser. (8:194)

Since the flow is decelerating as it passes through the diffuser, the adverse pressure gradient can cause the flow to separate. Bower (4:3,4) describes the impact of an adverse pressure gradient on diffuser flow as follows:

> At the entrance plane of the duct, the boundary layer, which is generally turbulent, is relatively thin, and the velocity profile is typical of the 1/7 power law variation. As the airstream moves against the adverse pressure gradient, which is nearly constant across any section of the boundary layer, it is retarded by the force of the pressure gradient and by friction at the bounding wall. When the momentum of the boundary layer is no longer able to overcome these forces and the fluid near the wall is brought to rest, the boundary layer separates. At the point of separation, the wall shear stress vanishes, and the inflection point appears in the boundary layer velocity profile. As the flow continues to oppose the adverse pressure gradient, the fluid near the wall begins to flow in the opposite direction to the mainstream.

Tests conducted on two-dimensional diffusers were done throughout the 1900's for a variety of divergence angles and values of (L/W). The results were compiled by Kline and are presented in Figure 6 (15:394). This figure shows the relationship between divergence angle and pressure recovery for different values of diffuser aspect ratio. Also plotted on this figure are curves of ideal pressure recovery in order to provide a graphical representation of diffuser efficiency and performance.

For this investigation, the ramp divergence angle was 10 degrees. In order to use Figure 6, the angle between divergent sides is twice that angle, or 20 degrees. Knowing the aspect ratio of the diffuser, one could predict the expected C_p value. Of immediate notice is the fact that at 20 degrees, the C_p values are well below the ideal values. This

means that there are significant losses occurring in this particular diffuser design and that efficiencies will be relatively low. This should be expected when the pressure data is reduced.

Because separation in a diffuser is associated with significant losses, a diffuser in which separation has been delayed should experience an associated decrease in losses. This should manifest itself in a less severe adverse pressure gradient and a higher value of pressure coefficient. It is hypothesized that the addition of riblets to a subsonic, straight-walled diffuser should not only delay flow separation but also increase and improve the pressure recovery.

III. Experimental Apparatus

Wind Tunnel

The experimental research for this thesis was conducted in the AFIT Nine-Inch Wind Tunnel Facility located in Building 19, Area B, of Wright Patterson AFB. The facility consists of a low speed, open circuit, draw-down tunnel and its 24-volt supporting power supply. The wind tunnel test section had a 9 inch by 9 inch square cross section and was 37 inches long. The floor and ceiling of the test section were constructed of wood and the side panels were made of plexiglass. Both side panels were hinged at the top and swung upward for easy model access. Fourteen circular instrumentation access ports, spaced 2.5 inches apart, were located along the centerline of the test section ceiling. Seven circular access ports, spaced 5 inches apart, were located along the section floor. The ceiling and floor ports had diameters of 1.5 and Ø.25 inches, respectively.

Tunnel static pressure, P_s, was measured using an inclined water manometer. The manometer was attached to three manifold pressure ports located at the midpoint of each side tunnel wall and the bottom wall, 1Ø.Ø inches from the beginning of the test section. The area at this location was the same as the test section. A static tube was used to confirm that this sidewall pressure, P_{sw}, was uniform across the tunnel width. The relation

$$P_{sw} = P_s \tag{11}$$

was used to determine the tunnel static pressure. A Pitot tube was inserted at this location to measure the total pressure. Flow velocities in the tunnel (previously measured) ranged from an idle speed of approximately 20 ft/sec to a maximum of almost 70 ft/sec. Because of the relatively slow velocities involved, Bernoulli's equation for incompressible flow, neglecting the gravity terms

$$P_T = P_S + 0.5\rho U^2 \tag{12}$$

where: P_T = tunnel total pressure

ρ = air density

U = freestream velocity

was quite acceptable. Solving Eq (12) for velocity resulted in:

$$U = \{2(P_T - P_s)/\rho\}^{1/2} \tag{13}$$

which was the equation used to determine the tunnel freestream velocities. The density was calculated using the ideal gas law relationship:

$$\rho = P_S/RT \tag{14}$$

where R = gas constant

T = tunnel temperature

Tunnel temperature was measured using a digital thermometer placed in the aft end of the test section. Adiabatic flow was assumed throughout

the tunnel flow area. Measurement readings were accurate to one tenth of a degree, Fahrenheit. The atmospheric pressure, P_{atm}, was recorded in inches of mercury, from a wall-mounted barometer located in the vicinity of the wind tunnel. The maximum velocity recorded during experimentation was 65 ft/sec.

Anemometry/Pitot Tube System

A hot film anemometry/Pitot tube system was critical to the successful completion of this work. Specifically, hot film anemometry was used to determine the characteristics of the freestream flow (i.e., laminar vs. turbulent) and additionally, as a check on the accuracy of the pressure readings taken from the ramp static ports for both the smooth and riblet ramp surfaces.

The anemometry system consisted of an IFA 100/200 System Intelligent Flow Analyzer, Model 1218-20 Hot Film Boundary Layer Probes, and an 18-inch single sensor anemometer probe holder with associated traversing mechanism. All equipment was manufactured by Thermo-Systems Inc., (TSI). The IFA 100/200 system provided both probe calibration and data acquisition and reduction software programs that related output bridge voltages to flow velocities. The Model 1218-20 probe was a hot-film type sensor with a platinum filament measuring 0.002 inches in diameter. This particular probe was constructed with a small metal rod extending from its base to protect the hot-film filament from contacting the body surface. The distance from the end of the rod to the platinum filament measured 0.005 in. An 18-in. probe holder was used to connect the hot-film probe to the IFA 100/200 system. The

probe holder was part of a manual traversing mechanism which was inserted into any of the 14 access ports on the top of the test section. Design of the traversing mechanism allowed the probe to be inserted normal to ramp at any access port location. The mechanism employed a vernier scale to allow highly accurate measurement and control of the probe-to-surface distance to within 0.001 in.

The Pitot tube was custom designed to provide extremely accurate total pressure measurements with minimal flow disturbance. The inside diameter of the probe measured 0.021 in. while the outside diameter measured 0.040 in. The probe was designed to utilize the same traversing mechanism as the anemometry system and therefore, provide "same location" total pressure information. The Pitot tube was connected to a 2-inch inclined water manometer with the other end open to atmospheric pressure.

Tunnel Model

One tunnel model was employed in this thesis with four basic modifications. The adjustable diffuser section actually represented one-half of a diffuser with the tunnel ceiling representing the flow centerline. Therefore, the relevant diffuser throat height parameter used throughout this text was H, where W=2H.

The basic model was constructed of wood. It was 36.0 in. long, 8.9 in. wide, and had a varying thickness. From the leading edge to an axial distance of 7.0 in., the diffuser section thickness had an elliptical shape varying from 0 to 3.75 in. At an axial distance between 7.0 in. and 15.0 in., the model had a constant 3.75 in. thickness. This was

defined as the diffuser throat section. At an axial distance of 15.0 in. a removable, diverging ramp began, providing a constant θ of 10 deg. The ramp extended from 15.0 in. to the length of the diffuser section--36.0 in. A side view of the diffuser model is shown in Figure 7.

In the experiment conducted by Martens in 1988, it was discovered that a pair of vertical vanes was needed on the diffuser model in order to generate separation. These vanes served to shield the model test section from, "highly vortical wall boundary layers as well as reinitializing the boundary layer on the vane surface" (17:28). Instead of the cardboard vanes used in the 1988 work, several pairs of 0.125 in. thick plexiglass vanes were constructed and bolted to the model, one inch from each wall. Each pair of vanes covered the length of the diffuser ramp, projected 5.5 in. into the throat section, and extended from the model surface to the tunnel ceiling. One pair was constructed for each throat height, H, investigated. Plexiglass was chosen for two reasons. First, it provided much more rigidity and stability during high speed runs. Second, it provided clear, unobstructed viewing into the test section during data runs. This proved invaluable during the anemometry/Pitot tube data acquisition runs where both the hot-film and Pitot tube came in close contact with the model surface.

Wood blocks were used beneath the model to adjust its height within the tunnel (corresponding to a change in H). Each of these blocks was 36.0 in. long and 8.9 in. wide. A rectangular section approximately 30.0 in. by 6.0 in. was removed from each block to accommodate the model instrumentation. The thicknesses of the blocks were 0.125, 0.250, 0.500, 1.00 and 1.50 in. The model was bolted to these support blocks during test runs to prevent movement during data acquisition.

The four modifications to the model involved the removable diffuser ramp. As stated previously, the ramp extended from an axial distance of 15.Ø in. to the diffuser exit. The first ramp was constructed of aluminum and measured 21.1Ø in. long, 8.9 in. wide, and Ø.125 in. thick. It was held in place with 12 machine screws. Prior to any data run, the screw holes were filled in with modeling clay and scraped flush. Fourty-one static ports were drilled along the ramp centerline, beginning one-half inch from the diffuser throat position and continuing every one-half inch. Each static port had a Ø.Ø21 in. diameter opening. The second ramp was merely a modification to the first. A thin strip of 3M Brand Fine Line Automotive Tape was used to cover the static ports. This was done in order to isolate the influence of any irregularities in the construction of the static ports on the flow behavior. These two ramps were referred to as smooth diffuser surfaces.

The third modification was a new ramp, measuring 21.1Ø in. long, 8.9 in. wide and Ø.125 in. thick that had riblets machined into the surface. The riblets measured Ø.Ø35 in. from peak-to-peak and from peak-to-valley and extended along the entire width and length of the ramp. This dimension was shown previously to be ideal for this investigation. In order for the riblets to be effective, the peak-to-valley dimension (Ø.Ø35 in.), needed to extend into the viscous sublayer. In other words, the riblet height needed to be superimposed on top of the smooth surface ramp. Since the thickness of both the smooth and riblet ramps were the same (Ø.125 in.), the riblet ramp needed to be raised slightly. Thin pieces of Ø.Ø35 in. thick aluminum were placed beneath the riblet ramp to provide this slight modification. Due to some warping encountered during the machining process, two additional machine screws were

added to this ramp (total=14) in order to keep it securely fastened to the main model. Similar to the smooth surface, modeling clay was used to fill in the screw holes and scraped to match the riblet contours.

The last modification involved the drilling of static ports into the riblet surface, identical to those of the smooth ramp in dimension and location. This put the static port in the middle of a valley in the riblet design. Figure 8 portrays the position of the static port in relation to the riblet surface. Drilling of these ports was accomplished only after all of the data for the riblet ramp was obtained. These last two modifications were referred to as the riblet diffuser surfaces. To sum, two physical ramps were used for this study, a smooth and riblet surface. Each one had two variations, one without static ports and one with ports.

Several other pieces of equipment were used in the completion of this thesis. A Tektronix Model SC504 Oscilloscope was used to monitor and tune the frequency response of the hot-film apparatus. A Zenith Z-248 computer system was used in the data acquisition and reduction portion of the experiment. Finally, three Dwyer Instrument 2-inch inclined water manometers were used to record model pressures and control tunnel speed.

Computer Software

Three computer software programs were utilized during the course of this investigation. The TSI IFA 100/200 software programs automated all of the hot-film probe calibrations and data acquisition. Data files generated by this software were consolidated and plotted using a plot

package called "GRAPHER," which was written by Golden Software. All of the figures in this report were generated using this package. Draft and final copies of this report were prepared on a Vendex Headstart III personal computer using "Manuscript" by Lotus. All copies were printed using a Panasonic KX-P1124 24-pin letter quality printer.

IV. Experimental Procedure

The experiments performed in this thesis were divided into three distinct groups. The first involved calibration of both the wind tunnel and hot-film anemometry equipment. This was important in verifying turbulent flow at the diffuser throat and also in preparation for the extensive hot-film work that was to come. A complete discussion of this procedure is found in Appendix B. The second group of experiments was performed with the smooth surface diffuser. Flow separation locations and surface pressure distributions, both with and without static ports, were obtained. The final group of experiments was performed with the riblet surface diffuser. Again, flow separation locations and surface pressure distributions were obtained with and without static ports. Because of the similarities involved with the last two groups of experiments, the details are presented below.

Data Collection Reference Parameters

Recall, from the Theory Section, that the prescribed height of the riblets was determined to be approximately 0.035 in. Martens (17:27), verified this value experimentally. Diffuser throat velocities used in that set of experiments ranged from 19.0 ft/sec to 51.0 ft/sec. This provided non-dimensional riblet heights, h^+, between 14.5 and 38.1 (17:32). The upper velocity was limited so as not to dislodge the installed cardboard vanes (discussed previously). Since the vanes in this experiment were of sturdier construction, the upper limit on velocity was extended to 61 ft/sec in order to determine the effectiveness of

riblets well outside the accepted h^+ range of 8 to 30. The lower limit of 19.0 ft/sec was not used in this test due to the inability to achieve stable flow at the diffuser throat. It was decided to use the remaining velocities from the Martens experiment to provide a basis for comparison. Table 1 shows the four chosen velocities and approximate h^+ values.

Table 1. U_{th} and h^+ Values Used for Data Acquisition

U_{th} (ft/sec)	h^+
29	21.9
39	29.5
51	38.1
61	47.5

The only other data collection reference parameter was the diffuser throat height, H. Martens used values of H ranging from 1.75 in. to 4.25 in. At values less than 1.75 in. inconsistent flow separation locations were noticed and confirmed in this work. At 4.25 in., the flow remain attached for all values of throat velocity. Because of this, H values of 1.75, 2.25, 2.75 and 3.25 in. were selected. These corresponded to those geometries investigated by Martens and provided excellent comparative data for this investigation.

Smooth Diffuser Tests

Prior to taking any data, turbulent flow needed to be established at the entrance to the diverging ramp. Initial boundary layer surveys using hot-film anemometry showed that laminar flow existed across the width of the channel. This was the same problem encountered by Martens. To alleviate this, a 0.75 in. wide strip of Number 120 grit sandpaper was attached to the diffuser throat, 7.0 in. upstream from the ramp divergence point. This served to artificially trip the boundary layer and cause transition to turbulent flow. Subsequent boundary layer surveys at the divergence point showed completely turbulent flow as seen in Figure 9. The 1/7 Power Law solution for turbulent flow over a flat plate is presented along with the Blasius laminar boundary layer solution. It was quite evident from the figure that turbulent flow did exist at the entrance to the expanding channel. Similar profiles were generated for the other geometries and throat velocities investigated. In all cases, turbulent flow was verified prior to any data acquisition.

The first series of tests conducted with the plain surface diffuser involved determining the flow separation point. This was accomplished using two different methods, Dow Corning 200 Fluid oil drops and tufts of string. For a given throat height and velocity, oil drops were applied to the diffuser throat area and also the diverging ramp section. The throat velocity was set and the resulting oil drop flow pattern allowed to develop for approximately two minutes. The throat speed was then brought to rest and the separation location noted and recorded. The ramp was then cleaned with a mild solution of alcohol and water and the test repeated two more times. The average of the three data runs

was determined and recorded. This sequence was repeated over the range of velocities and throat heights described earlier. Accuracy of this method was valid to within Ø.1 in.

As a check on the oil drop method, similar tests were run using tufts of string. Numerous tests were conducted with various configurations and lengths. It was determined that thin tufts, approximately one inch in length, facing rearward, worked best. Only one row of tufts was used in order to minimize the disturbance to the flow. The tufts were attached to the ramp surface parallel to the flow direction using a Ø.25 in. wide piece of Scotch tape. The last quarter inch of the string was frayed--this provided the most dramatic indication of flow visualization. The row of tufts was moved up and back in the vicinity of the separation point determined from the oil drop analysis until separation was observed. Separation was indicated when the frayed portion began to flutter violently from side to side. Again, three runs at each velocity and throat height were obtained and averaged. Accuracy with this method was again valid to within Ø.1 in. This series of tests was run for the smooth diffuser surface, first for the ramp with static ports and second, for the ramp without ports (i.e., static ports covered with tape) to determine if the addition of the ports had any effect on the separation location. Boundary layer surveys both upstream and downstream of the observed separation location were performed for several data points in order to verify the existence of separated flow.

The second series of tests involved collection of ramp surface pressures. These tests were conducted two separate ways. First, with the static ports uncovered, the relevant throat heights and velocities were adjusted and the corresponding throat and ramp surface pressures

recorded. Pressures were measured using a 2-inch inclined water manometer, with one end open to atmospheric pressure, the other end successively connected to each ramp pressure port. The manometer was allowed to stabilize for one minute at each pressure port prior to the data being recorded. Each throat height/velocity combination was accomplished three times and a simple average obtained. Accuracy of manometer readings was valid to within 0.005 in. H_2O.

In order to determine whether or not the presence of the pressure ports affected the flow, the ports were then covered with fine line tape and the test reaccomplished. This time, the pressures were obtained using a hot-film and Pitot tube. The access ports along the top of the test section allowed the pressure to be obtained along the ramp centerline location in order to provide a comparison to the static port-derived pressures. This complete procedure may be found in detail in Appendix C. The hot-film probe was cleaned with methanol after each series of runs and allowed to air dry. Again, each data run was accomplished three times and an average derived.

Riblet Surface Diffuser Tests

The riblet surface tests were done similar to the smooth surface tests. The surface without static ports was investigated first with the following exception: oil drops could not be used on the riblet surface as a means of determining flow separation. The riblet material caused a capillary-like effect and began to streak the oil drops prior to any airflow. This was expected based on the work by Martens and Wieck (17:36; 22:27). Since excellent results were obtained using the one inch

tufts for the plain surface, they were used for the riblet surface. Only one row of tufts was used and each was applied to the peak of the riblet surface with Scotch tape. Figure 10 shows how the string tufts were applied to the riblet surface. Since no analytical prediction technique existed for determining flow separation over a riblet surface, this single row of tufts was moved upstream from the rear of the diffuser ramp until separation was observed. The vigorous flutter noticed for the plain diffuser case was also evident for the riblets and was used as the determining factor in estimating the separation point.

Riblet surface pressure data was obtained similar to the smooth surface diffuser. The hot-film/Pitot tube combination was used to collect data at each throat geometry/velocity combination.

With the riblet surface data in hand, static ports were machined into the ramp, taking care not to create any anomalies or burrs that would alter the flow above and beyond that caused by the riblets themselves. The plate was reattached to the model and separation and pressure data obtained as in the smooth diffuser tests.

V. Results and Discussion

These experiments were designed to determine the effect of riblets on the pressure recovery in a straight-walled diffuser. Previous tests showed significant delays in flow separation due to riblets and this seemed a logical starting point from which to launch an investigation into the changes in diffuser surface pressure distributions.

Diffuser Separation Data

Once turbulent flow at the diffuser throat was verified, data collection involved recording the throat height, H, the throat velocity, U_{th}, and the location of flow separation, X_{sep}. U_{th} was set using the hot-film and adjusting the tunnel speed so that an appropriate probe output voltage was achieved that corresponded to the desired throat velocity. X_{sep} was measured from the ramp divergence point along the ramp surface. Table 2 shows the diffuser ramp separation points for the smooth surface diffuser as a function of throat height and velocity. Throat velocities are given in (ft/sec), and throat heights and separation locations are in inches. Accuracy of separation location measurements was valid to within Ø.1 in. The separation points are given for the cases of no static ports (clean) and static ports (ports), and were calculated as follows:

$$X_{sep}\ (avg) = [X_{sep}\ (avg)(oil) + X_{sep}\ (avg)(tufts)]/2 \qquad (15)$$

where: X_{sep} (avg)(oil) = average of three runs using oil drops

X_{sep} (avg)(tufts) = average of three runs using tufts

and

$$X_{sep}\ (avg)(smooth) = [X_{sep}\ (avg)(clean) + X_{sep}\ (avg)(ports)]/2 \qquad (16)$$

Also provided is the value of separation location determined from the Stratford criteria. The difference between the average separation location and the Stratford-derived location is presented as a percent change. The percent change is determined using:

$$\%\ change = [X_{sep}\ (avg)(smooth)\text{-}Stratford]/Stratford \qquad (17)$$

Two trends are quite evident from the data in Table 2. First, the introduction of the static ports had a negligible effect on the separation location. Obviously, the mechanism driving separation in this diffuser design was not significantly influenced by the addition of these ports. Since the flowfield was not altered to any great extent, it was believed that the pressure recorded directly from these ports would accurately reflect the true surface pressure distribution.

The second trend is the excellent agreement with the predicted separation location using Stratford's criteria. In all cases, separation was predicted earlier than the visualization method indicated. This is a trend that was also seen in data presented by Cebeci and Smith

(5:378-384) and Martens (17:34-36). The larger percent errors occurred for the smaller throat heights and velocities (approximately 3 percent), decreasing to approximately 1.25 percent for the largest throat height.

Table 2. Diffuser Flow Separation Locations-Smooth Surface

U_{th}	H	X_{sep} avg clean	X_{sep} avg ports	X_{sep} avg smooth	Stratford	Percent Change
29	1.75	5.48	5.47	5.48	5.32	3.01
39		5.91	5.90	5.91	5.74	2.96
51		6.41	6.43	6.42	6.22	3.22
61		6.84	6.85	6.84	6.64	3.01
29	2.25	7.45	7.44	7.45	7.25	2.76
39		8.18	8.20	8.18	7.96	2.76
51		9.03	9.02	9.03	8.78	2.85
61		9.81	9.80	9.81	9.54	2.83
29	2.75	9.70	9.69	9.70	9.42	2.97
39		10.73	10.74	10.73	10.42	2.98
51		12.04	12.04	12.04	11.80	2.03
61		13.75	13.76	13.75	13.48	2.00
29	3.25	11.92	11.91	11.92	11.74	1.53
39		13.39	13.40	13.38	13.18	1.52
51		15.98	15.98	15.98	15.75	1.46
61		18.50	18.49	18.50	18.28	1.20

Table 3 shows the diffuser ramp separation points for the riblet surface as a function of throat height and velocity. Average values for X_{sep} are calculated using three runs for the tuft case only, since oil drops could not be used on this surface. An X_{sep} entry of 21.00 indicates no flow separation. The average riblet surface separation distance was defined as follows:

$$X_{sep}\ (avg)(riblet) = [X_{sep}\ (avg)(clean) + X_{sep}\ (avg)(ports)]/2 \qquad (18)$$

It is interesting and important to note that the addition of the static ports had no effect on the separation point. This was similar to the result obtained for the smooth surface ramp. The mechanism driving separation in the riblet surface ramp appears unaffected by the addition of these particular size static ports. If the flowfield is not significantly altered, then an accurate surface pressure distribution was believed possible by direct readings from the static ports.

Table 3. Diffuser Flow Separation Locations-Riblet Surface

U_{th}	H	X_{sep} avg clean	X_{sep} avg ports	X_{sep} avg riblet
29	1.75	18.23	18.22	18.22
39		19.45	19.48	19.47
51		19.65	19.67	19.66
61		20.00	20.03	20.01
29	2.25	18.33	18.30	18.32
39		19.50	19.54	19.52
51		19.71	19.74	19.73
61		9.81	9.79	20.33
29	2.75	18.66	18.64	18.65
39		19.54	19.56	19.55
51		19.75	19.76	19.75
61		13.75	13.76	20.55
29	3.25	18.71	18.70	18.70
39		19.61	19.62	19.62
51		19.82	19.83	19.83
61		21.00	21.00	21.00

The data in Tables 2 and 3 are combined in Figure 11 which shows the diffuser ramp separation locations as a function of diffuser aspect ratio for both the smooth and riblet surface cases. The separation locations plotted are the averages of all runs (column 5 for Tables 2 and 3). This figure correlates very well to the results presented by King (12:5). It is obvious that separation occurs farther downstream for the riblet surface ramp compared to the smooth surface for any aspect ratio and velocity. Also, as the velocity increases, the separation location moves farther downstream for both the riblet and smooth surface ramps, although this change is more pronounced for the smooth surface. Interestingly, the separation location for the riblet surface appears to be relatively geometry independent--a result noticed by King and verified here.

A plot of $\Delta X_{sep}/X_{sep}$ as a function of aspect ratio and velocity is found at Figure 12. It can be seen that for high aspect ratios (less stable flows) the percent change in separation location is higher than for the smaller aspect ratios (more stable flows). As King puts it, ". . .viewed another way, a diffuser which is more likely to stall will be helped proportionately more by riblets. . ." (12:5).

Diffuser Pressure Data

At each throat height and velocity, the ramp surface pressure was obtained two ways. The first involved use of the hot-film/Pitot tube combination discussed earlier. The second method involved reading the static pressure (referenced against atmospheric pressure) from a manometer connected directly to static ports of the ramp itself. Figure 13

shows typical results from data runs at two different geometries and velocities. Similar graphs were generated for each geometry and velocity for both the smooth and riblet surfaces. It was evident that valid pressure data was attainable for both types of surfaces using either method. The riblet data appeared to substantiate the earlier result that the addition of static ports to the riblet ramp had no effect on the separation location. Because the separation location did not change, no change in the surface pressure distribution was expected. Since each method yielded similar pressure distributions, only the manometer-derived pressures, averaged over three runs, is presented in this thesis in Appendix E.

Data Analysis

For comparison purposes, the raw data, given as ($P_{static} - P_{atm}$), were converted to a pressure coefficient, C_p, using

$$C_p = (P_{static} - P_{static\,throat})/q_{throat} \tag{19}$$

where

$$q_{throat} = 0.5\rho_{throat}(U_{throat})^2 \tag{20}$$

The effect of Eq (19) was to reference all the data to conditions at the diffuser throat where the pressure coefficient would reduce to a zero value.

The pressure coefficients for each geometry and velocity investigated were plotted against a non-dimensional ramp distance, determined by dividing the ramp pressure location, measured along the ramp from the minimum pressure point, by the ramp length. The results are plotted in Figures 14 through 17. Also plotted on each figure is the line of ideal pressure recovery, discussed previously.

Immediately apparent from each figure is the fact that for any aspect ratio or velocity, riblets improved the overall pressure recovery over that of the smooth surface ramp. Because the separation location was moved rearward in each instance, the associated increase in pressure recovery was expected.

The second trend from these figures was the distinctive flat region in the smooth surface curves. Beyond the minimum pressure point, the C_p values rose sharply to a maximum and then remained constant at that maximum value. The value to which the curves rose was slightly dependent on velocity. The ramp location at which the curve went flat was close to that observed with the visualization techniques. Upon close inspection of the riblet pressure data, a similar trend was observed. Although the shape of the C_p curve for riblets was noticeably different than for the smooth surface, the C_p values increased to a maximum (different than the smooth surface maximum) and then remained constant. Because separation on the riblet surface was occurring towards the end of the ramp for all geometries and velocities, it was difficult to establish whether the C_p curve would remain flat. Therefore, for the riblet case, no definite criteria could be established as to the point of separation. However, for the smooth surface, the separation C_p and its location were

determined at the point where the curve remained flat. This point was clearly evident and easily discernible and compared favorably to that location determined using visual means.

The fact that the C_p curves remained flat after flow separation implied that the flow on the ramp surface, in the vicinity of the static ports, did not reverse direction or reattach. Apparently, as the flow separated, it remained separated and well-behaved. Any reattachment or reverse flow would have shown up as a change in the "flat region" C_p where none was noted. Additionally, during the oil drop experiments, the circular oil drops streaked in the direction of flow up until the separation point, after which they remained circular. Any flow on the surface would have streaked the oil drops and again, no streaking was noticed downstream of the separation point. Therefore, this trend in the C_p data was quite reasonable.

Also apparent is the fact that all the velocity curves, for both the smooth and riblet surfaces, lie fairly close to one another. Due to the scaling of the figures, it is difficult to note any difference. However, close inspection of the reduced C_p data reveals a slight increase in the separation C_p value for increasing velocity. This trend was equally noticeable for the smooth surface and riblet curves. However, in both cases, the difference in C_p between the lowest and highest velocities never varied more than approximately 3 percent.

A final trend in the figures involved the slopes of the C_p curves immediately after the ramp divergence point. As the aspect ratio of the diffuser increased, the slope of the smooth and riblet surface C_p curves increased. This was easily explained by the fact that as the aspect ratio went up, the rate of area increase went up also and the diffuser became

more susceptible to stall (higher L/W). This implied a higher adverse pressure gradient and was seen as a larger slope on the C_p curves. Additionally, for a given aspect ratio, there was a significant difference between the smooth and riblet surface C_p curves which became more pronounced at the higher aspect ratios. This was due to the fact that at the higher aspect ratios, the diffuser was subjected to a much more severe adverse pressure gradient. Since riblets delayed the onset of separation, the pressure gradient was made less severe and therefore the slope of the riblet C_p curve lower. Since the separation point for the riblet surface was not varying over the range of geometries and velocities investigated, the shape of the C_p riblet curve remained fairly constant. However, for the smooth surface ramp, the separation location moved farther downstream as the aspect ratio was decreased. This implied a less severe pressure gradient (not favorable however) and a lower slope. This shows up in the figures as a noticeable difference between the smooth and riblet surfaces for the higher aspect ratios and a less pronounced deviation at the lower ones.

As stated previously, for all geometries and velocities investigated, the addition of riblets to the smooth surface diffuser improved the pressure recovery at the diffuser exit. These pressure coefficients were converted to an efficiency factor using Eq (8). As stated previously, it defines diffuser performance as the percentage of the pressure recovery obtained as compared to that of an ideal diffuser experiencing no total pressure or skin friction losses. Figure 18 displays diffuser efficiency as a function of aspect ratio. Interestingly, the efficiency appears to relatively independent of both geometry and velocity for both the smooth and riblet surfaces.

An estimate of the diffuser efficiency, for comparison purposes, can be made by referring to Figure 6. The aspect ratios of the diffuser used in this experiment ranged from 3.Ø3 to 5.63. The total included angle 2θ, was 2Ø degrees. Using the Reid 5.5 aspect ratio data, a reasonable estimate of the expected pressure coefficient for this diffuser was made. Unfortunately, Reid's data is only plotted for divergence angles between 7 and 17 degrees. However, by extrapolating the data to 2Ø degrees, the pressure coefficient was estimated to be approximately Ø.5. This compared favorably to the measured pressure coefficient for the highest aspect ratio diffuser (5.63) used in this experiment. The efficiency calculated from Figure 6 data was 56 percent and this compared well with the experimental efficiency of approximately 52 percent.

Unfortunately, no data for aspect ratios smaller than 5.5 were available. However, close examination of the trends in Figure 6 show that smaller aspect ratio diffusers will have lower pressure coefficients. Examining the measured pressure coefficients, this trend was verified. The lower aspect ratios have proportionately lower ideal pressure coefficients and so the overall efficiency of the diffuser remained fairly constant at 52 percent.

The riblet results seem to follow the same trend, providing an approximate 35 percent increase in diffuser efficiency. The most improvement seems to occur for the high aspect ratio geometry (most severe stall) and the least for the lower aspect ratio. This appears to match the earlier separation result noted by King and Martens that riblets appear to be most effective in those conditions most likely leading to stall. An important point to be made here is that not only are riblets effective in delaying flow separation in turbulent, adverse

pressure gradients, but they also appear to alter the pressure distribution in a favorable manner that provides improved pressure recovery at the same time.

Because Figure 18 shows very little dependence on velocity, a new graph was made that plotted diffuser efficiency as a function of throat Reynolds number, determined as follows

$$Re_d = (U_{th} D_h)/\nu \tag{21}$$

where: D_h = 4(throat area)/(throat perimeter)

The hydraulic diameter, D_h, is a parameter commonly used in calculations to eliminate the dependence of geometry in engineering problems. It is also used to normalize the viscous effects of a boundary layer growing on the interior of a duct of arbitrary shape to that of one growing on the interior of a circular duct. The throat area and perimeter were well-defined values that varied with aspect ratio. Reynolds numbers based on this criteria ranged from 40,000 to approximately 140,000.

Figure 19 shows the relationship of diffuser efficiency to the throat Reynolds number. It is evident from this figure that the effect of throat Reynolds number on diffuser efficiency appears to be relatively minor in the range investigated. This was expected from the smooth surface and appears to be true for the riblet surface as well.

VI. Conclusions and Recommendations

Conclusions

As a result of this investigation into the effect of riblets on the pressure recovery in a straight-walled diffuser, the following conclusions were made:

1. Riblets, in addition to significantly delaying flow separation in a diffuser, also altered the pressure distribution in a manner that allowed for improved pressure recovery. The amount of this improvement was an increase in the pressure coefficient between 30 and 38 percent over what was expected from a diffuser of the design used in these experiments. This result appeared valid for any combination of geometry or velocity with the most improvement occurring for the condition most likely leading to stall.

2. Inherent in an improvement in the efficiency of the diffuser with riblets is a reduction in the aerodynamic and skin friction losses. Although the skin friction losses were not measured, it may be inferred that an improvement in diffuser efficiency should result in a reduction of these loss mechanisms. Riblets were shown to significantly delay flow separation and this delay in separation resulted in a noticeable increase in the diffuser efficiency as compared to the smooth surface diffuser.

3. The effect of riblets on the surface pressure distribution appeared to be insensitive to the range of geometries and velocities investigated in this experiment. Because of the relatively small range of aspect ratios investigated, the change in efficiency due to changes in

geometry for the smooth surface diffuser was not expected to be significant. It appeared that the same result held for the riblet surface diffuser.

4. The introduction of static ports into the riblet surface did not appear to influence the effect of the riblets on flow separation or surface pressure distribution. The flow separation points and pressure distributions obtained for the riblet surface with and without static ports were similar along the ramp centerline. This indicated that whatever mechanism inherent in the riblet shape was influencing the diffuser flow, was not disturbed appreciably by the presence of the static ports.

Recommendations

This thesis revealed an obvious benefit in using riblets in a subsonic straight-walled diffuser to delay flow separation and increase pressure recovery. The following additional areas are recommended for follow-on study:

1. Most data on diffusers is presented for varying divergence angles. This model allowed only one angle, namely 20 degrees. An investigation into the effect of riblets on flow separation and pressure recovery enhancement should be conducted over a range of divergence angles.

2. Measured boundary layer thicknesses were on the order of 0.2 to 0.3 in. At the larger aspect ratios, this was almost 20 percent of the throat height and prevented any separation data from being obtained at throat values less than 1.75 in. A smaller throat height would have allowed a greater range of aspect ratios to be investigated. A variable

geometry ramp, or several different geometry ramps, would allow an investigation into changes in ramp divergence angle, along with aspect ratio, on diffuser performance.

3. Although the riblets improved the overall performance of the diffuser for any combination of geometry or velocity, the smooth surface diffusers appeared to give equal or better performance out to their separation points. More work into this phenomenon needs to be accomplished in order to fully understand the effect riblets have on pressure recovery.

4. In these experiments, the entire length of the ramp was machined with riblets. An investigation into the effect of a ramp that is partially machined with riblets might provide insight into the mechanism that allows riblets to delay flow separation and improve pressure recovery.

5. The diffuser used in this work was designed to give poor pressure recovery (i.e., on the order of 50 percent) in order to determine the effectiveness of riblets in delaying flow separation and enhancing pressure recovery. An investigation into the effect of riblets on the flow separation and pressure recovery in a well-designed diffuser might prove useful.

6. The static ports used in this investigation were machined to provide the minimum disturbance to the flow. Any altering of the surface has the potential to disturb the oncoming flow and hence disrupt and possibly cause separation. An investigation into the effect of static port size and its effect on riblet performance would provide important insight.

References

1. Anders, John B. and others. "The Fix for Tough Spots," Aerospace America, 26: 24-27 (January 1988).

2. Bacher, E.V. and C.R. Smith. "Turbulent Boundary-Layer Modification by Surface Riblets," AIAA Journal, 24-8: 1382-1384 (August 1986).

3. Barna, P.S. Fluid Mechanics for Engineers (Third Edition). New York: Plenum Publishing Corporation, 1969.

4. Bower, William W. "An Analytical Procedure for the Calculation of Attached and Separated Subsonic Diffuser Flows," Proceedings of the AIAA/SAE 10th Propulsion Conference. Paper No. 74-1173. New York: American Institute of Aeronautics and Astronautics, 1974.

5. Cebeci, Tuncer and A.M.O. Smith. Analysis of Turbulent Boundary Layers. Orlando: Academic Press, 19[illegible].

6. Chang, Paul K. Separation of Flow. Elmsford NY: Pergamon Press, 1970.

7. Gibson, Arnold H. Hydraulics and its Applications (Fifteenth Impression). London: The Whitefriars Press Ltd., 1947.

8. Hill, Philip G. and Carl R. Peterson. Mechanics and Thermodynamics of Propulsion. Reading MA: Addison-Wesley Publishing Company, 1965.

9. Hinze, J.O. Turbulence (Second Edition). New York: McGraw-Hill Book Company, 1975.

10. IFA 100 and IFA 200 System Intelligent Flow Analyzer Instruction Manual (Revision C). Thermo-Systems Incorporated, St. Paul MN, August 1987.

11. Karamcheti, Krishnamurty. Principles of Ideal-Fluid Aerodynamics (Reprint Edition). Malabar FL: Robert E. Krieger Publishing Company, 1980.

12. King, Paul I., Nathan W. Martens and Milton E. Franke. "Effect of Riblets on Flow Separation in a Subsonic Diffuser," Forum on Turbulent Flows, Proceedings of the 3rd Joint ASCE/ASME Mechanics Conference, La Jolla, CA, (July 1989) (submitted to Jnl Fl Engr, review pending).

13. King, Paul I. Personal Communication. School of Engineering, Air Force Institute of Technology (AU), Wright-Patterson AFB OH, 15 June-15 November 1990.

14. Kline, Stephen J. "On the Nature of Stall," Transactions of the ASME, Series D: Journal of Basic Engineering, 81-3: 305-320 (September 1959).

15. Kline, Stephen J., D.E. Abbott, and R.W. Fox. "Optimum Design of Straight-Walled Diffusers," Transactions of the ASME, Series D: Journal of Basic Engineering, 81-3: 320-331 (September 1959).

16. Kuethe, Arnold M. and Chuen-Yen Chow. Foundations of Aerodynamics: Bases of Aerodynamic Design (Third Edition). New York: John Wiley and Sons, 1976.

17. Martens, Nathan W. Effect of Riblets Upon Flow Separation in a Subsonic Diffuser. MS Thesis, AFIT/GAE/AA/88D-23. School of Engineering, Air Force Institute of Technology (AU), Wright-Patterson AFB OH, December 1988.

18. Mattingly, Jack D., William H. Heiser and Daniel H. Daley. Aircraft Engine Design. New York: American Institute of Aeronautics and Astronautics, 1987.

19. Reidy, L.W. And G.W. Anderson. "Drag Reduction for External and Internal Boundary Layers Using Riblets and Polymers," Proceedings of the AIAA 25th Aerospace Sciences Meeting. Paper No. 88-0138. New York: American Institute of Aeronautics and Astronautics, 1988.

20. Walsh, Michael J. "Drag Characteristics of V-Groove and Transverse Curvature Riblets," Viscous Flow Drag Reduction. Progress in Astronautics and Aeronautics, Volume 72, edited by Gary R. Hough. Technical Paper from Symposium on Viscous Drag Reduction, Dallas TX, November 1979. 168-184. New York: American Institute of Aeronautics and Astronautics, 1980.

21. Walsh, Michael J. "Turbulent Boundary Layer Drag Reduction Using Riblets," Proceedings of the AIAA 20th Aerospace Sciences Meeting. Paper No. 82-0169. New York: American Institute of Aeronautics and Astronautics, 1982.

22. Weick, Timothy D. Effect of Riblets on Flow Separation From a Cylinder and an Airfoil in Subsonic Flow. MS Thesis, AFIT/GAE/AA/89D-40. School of Engineering, Air Force Institute of Technology (AU), Wright-Patterson AFB OH, December 1989.

Appendix A Equation Derivation

This appendix contains the detailed derivation of Eq (6) used to determine flow separation within the diffuser section as described in the Theory section. Stratford's relationship is written as

$$F(x) = C_p(x dC_p/dx)^{0.5}(10^{(-6)}R_x)^{(-.1)}$$

where:

C_p = pressure coefficient, $C_p = 1 - (U_e/U_\infty)^2$

x = flow location measured along ramp

dC_p/dx = pressure distribution

Re_x = Reynolds number, $Re_x = xU_e/\nu$

U_e = boundary layer edge velocity (ft/sec)

U_o = velocity at beginning of adverse pressure gradient

$F(x)$ = Stratford's separation criteria parameter

Stratford's relationship was simplified using the continuity equation for steady, one-dimensional incompressible flow and the geometry of the diffuser. The continuity equation is written as

$$A_oU_o = A_eU_e \tag{22}$$

where A_o = diffuser throat area (ft)

U_o = velocity at A_o location (ft/sec)

A_e = diffuser area at boundary layer location (ft)

U_e = boundary layer edge velocity at Ae location

Rearranging Equation 22 resulted in the following relationships:

$$A_e = (A_o U_o)/U_e \tag{23}$$

$$U_e = (A_o U_o)/A_e \tag{24}$$

A side view of the model is shown in Figure 20. From the figure the following geometric relationships were derived

$$A_e = H + x \sin \theta \tag{25}$$

$$A_o = H \tag{26}$$

$$dA_e/dx = \sin \theta \tag{27}$$

where H = diffuser throat height

θ = ramp divergence angle

To derive an expression for C_p in terms of x, the ideal pressure coefficient, $C_{p\,ideal}$ was used. The ratio (A_o/A_e) is easily shown to be:

$$A_o/A_e = H/(H + x \sin\theta) \tag{28}$$

This provides a relationship between C_p and x, which can be differentiated to obtain an expression for dC_p/dx:

$$dC_p/dx = (2H^2 \sin\theta)/(H + x \sin\theta)^3 \tag{29}$$

Finally, substituting all into the original Stratford expression yields:

$$F(x) = \{1 - H^2/(H + x\sin\theta)^2\}\{2xH^2 \sin\theta/(H + x \sin\theta)^3\}^{0.8}\{R_x 10^{(-6)}\}^{(-.1)} \tag{30}$$

Appendix B: Equipment Calibration Procedure

The first group of experiments conducted during this investigation involved the calibration of the wind tunnel and hot-film anemometry equipment. The purpose of this appendix is to explain the details of each calibration process.

Wind Tunnel Calibration

The wind tunnel calibration was a relatively simple process that involved the use of two water manometers, a digital thermometer and a barometer. The manometers were used to measure the total and static pressures in the tunnel, the digital thermometer to measure the temperature in the tunnel test section and the barometer to measure the atmospheric pressure.

It was previously shown that the tunnel sidewall pressure was equal to the tunnel static pressure. The sidewall pressure was an easily measured quantity and varied directly with increases and decreases in the tunnel speed. This quantity was therefore chosen as the control parameter in setting the tunnel speed. With the static and total pressures measured, a relationship between the static pressure and the tunnel q was possible. This relationship is plotted in Figure 21 for two different temperatures and pressures. It is evident from this figure that the tunnel q (defined as the difference between the measured total and static pressures), was independent of both temperature and pressure.

With this relationship established, it was a simple matter to derive the actual velocities on any given day by measuring the atmospheric pressure and temperature and using the following equation:

$$U = (2q/\rho)^{(0.5)} \tag{31}$$

All calibrations were of course performed with no obstructions in the tunnel.

Hot-Film Probe Setup

With the tunnel velocity determined, calibration of the hot-film could proceed. It was determined early in the experiment to calibrate the hot-film in the tunnel. This was done in order to calibrate the boundary layer probes in an environment duplicating the actual experimental conditions. This was felt necessary in order to reduce any possible error introduced by calibrating in an external flow.

Prior to any calibration, the instrumentation needed to be assembled. Detailed instructions for assembly of the equipment was contained in the IFA 100/200 System Instruction Manual (10:1-1 to 3-5). The system was constructed by connecting the probe holder to the IFA 100/200 setup. The IFA 100/200 combination was connected to a Zenith Z-248 computer system to aid in data acquisition and probe calibration. The hot-film probe was then inserted into the holder, thus completing the circuit. The probe holder was clamped to the traversing mechanism

and inserted into the wind tunnel at the calibration location, 10 inches upstream of the test section. The traversing mechanism was adjusted to position the boundary layer probe in the center of the tunnel.

Once the probe was in place, the 100/200 system operating parameters needed to be set. These parameters included the transducer, frequency response and signal conditioner. The formulation and input of these parameters is discussed in detail in the operating instructions. The transducer parameters consisted of the cable resistance and the probe operating resistance. The cable resistance was measured first and input to the IFA 100. Its value was then automatically subtracted from all future readings. The probe resistance was measured next and compared to the factory specifications on the shipping container to determine the probe's validity. If a probe proved worthy, its operating resistance was manually input using the IFA 100 and the calibration procedure continued.

The frequency response of the circuit was then adjusted by setting the system to RUN, applying a square wave test signal and observing the output on an oscilloscope. This procedure was done with the tunnel adjusted to its highest operating speed. The frequency response was adjusted via bridge and cable compensation controls to produce the proper square wave test signal (10: Appendix 1), resulting in the optimization of the system.

The final set of parameters consisted of the offset, gain and filter controls. These parameters adjust the IFA 100/200 output signal to the specific needs and conditions under which the experiment was being conducted, and were set either manually or through the IFA 200 software.

Hot-Film Calibration

The procedure of calibrating the probe began with the insertion of the probe into the tunnel at the calibration station (10 inches upstream of the test section). Software provided with the IFA 200 System provided both probe calibration and data acquisition computer programs that were easy to use and quite helpful. This software was brought on line and appropriate information such as temperature, pressure and probe serial number were input. Once the software was ready to accept data, the tunnel was started and a velocity set via the sidewall static pressure. The tunnel was allowed to stabilize for one minute prior to any data being taken. The data was recorded as a bridge output from the hot-film probe and was fed directly to the Zenith computer system. Once the data was taken, the tunnel velocity was manually adjusted to the next velocity and the process repeated for the desired number of data points.

Once the raw data was collected, it was processed and reduced using the IFA 200 software. The probe calibration program plotted the output bridge voltage against the tunnel velocity and fit a fourth order curve fit to the data of the form:

$$E_b = A + B(U) + C(U)^2 + D(U)^3 + E(U)^4 \qquad (32)$$

where: E_b = probe output voltage (volts)

U = tunnel velocity (ft/sec)

A-E = anemometer constants

The anemometer constants were sensitive to changes in temperature. Due to the poor air conditioning in Building 19 and the relatively large fluctuations in the ambient temperature, calibration data was collected for a range of temperatures over which the experiment was conducted. This range was from between 69° F to 80° F. Calibration curves for this range were constructed and are plotted in Figure 22. The fourth order curve fit to the data was within less than one percent error at each point. The usefulness of the IFA 200 system was that once the calibration was performed, the constants and all pertinent data were stored in memory and it was a simple matter to recall the probe serial number during the data acquisition program and acquire data. The software would then reduce the output voltage and determine the flow velocity.

Appendix C Hot-Film/Pitot Tube Methodology

The purpose of this appendix is to describe the procedures used during the hot-film and Pitot tube data acquisition portion of the experiment. Specifically, the details involved with acquiring boundary layer surveys and the techniques used in determining the static pressure are discussed.

One of the basic assumptions in boundary layer theory is that the static pressure of the freestream airflow is transmitted through the boundary layer to the surface (16:299). In other words,

$$(dp/dy) = 0 \tag{33}$$

where y is measured normal to the surface over which the air is flowing. With this simple, but important assumption, the surface pressure distribution was obtained first by performing a boundary layer survey to determine the boundary layer thickness, δ, and edge velocity, U_e, and then inserting a Pitot tube at that location and measuring the total pressure. These values were used to calculate the static pressure using Eq (12).

Determination of Boundary Layer Thickness

As a precursor to measuring the total pressure, the boundary layer thickness needed to be determined. Most classical texts on boundary layer theory define the thickness of the boundary layer to be at that

point where the velocity in the boundary layer reaches 99 percent of the measured freestream value (16:306,311). Although this is conceptually satisfying, it is experimentally difficult to ascertain.

The boundary layer thickness was calculated in this thesis by applying Cole's wake function to each boundary layer survey. This expression was written as

$$u^{+} = \phi_1 y^{+} + \{\Pi(x)/\kappa\} w(y/\delta) \tag{34}$$

where:

u+ = dimensionless velocity parameter, u+ = U/U_τ

U = flow velocity in the boundary layer at y (ft/sec)

$\phi_1(y^{+})$ = turbulent boundary layer law of the wall function

$\Pi(x)$ = Cole's profile parameter

κ = von Karman's mixing length constant

$w(y/\delta)$ = Cole's wake function

If this equation is evaluated at y = δ, $\Pi(x)$ can be eliminated resulting in

$$U/U_\tau = (1/\kappa)\ln(yU_\tau/\nu) + c + \{U_e/U_\tau - (1/\kappa)\ln(yU_\tau/\nu) - c\}\sin^2\{\pi y/(2\delta)\} \tag{35}$$

where:

y = local vertical height (ft)

c = Cole's integration constant with a value between 4.9 and 5.5

δ = boundary layer thickness (ft)

There are two unknowns in this equation, U_e and δ. Solving for U_τ can be done by minimizing the root-mean-square of the all the data errors. All terms in Eq (35) were moved to the right hand side of the expression and set equal to an error parameter, ϵ. A value of δ was then guessed, and a range of U_τ was used with the boundary layer data to produce a corresponding range of ϵ values. Taking the square root of the sum of the squares of ϵ produced a value proportional to the root-mean-square error (ϵ_{rms}) for the chosen δ. This procedure was performed for a number of different boundary layer thicknesses, a graph generated of U_τ vs. ϵ_{rms}, and the minimum value of each $\epsilon_{rms} - U_\tau$ curve connected. The minimum value on this new curve represented the δ corresponding to the smallest ϵ_{rms}.

With δ determined, the Pitot tube was inserted into the flow at that location and the total pressure measured. With the velocity measured via the hot-film, and the total pressure measured with the Pitot tube, the static pressure was calculated using Eq (12).

Appendix D Figures

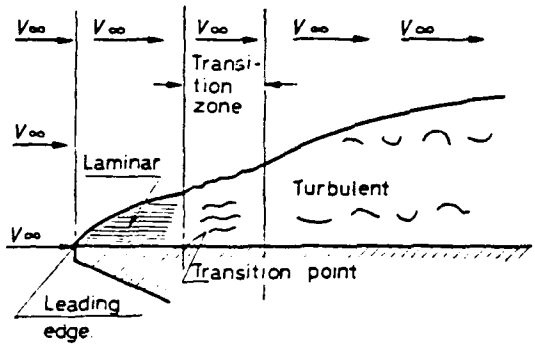

Figure 1. Laminar and Turbulent Boundary Layers (Flat Plate) (3:170)

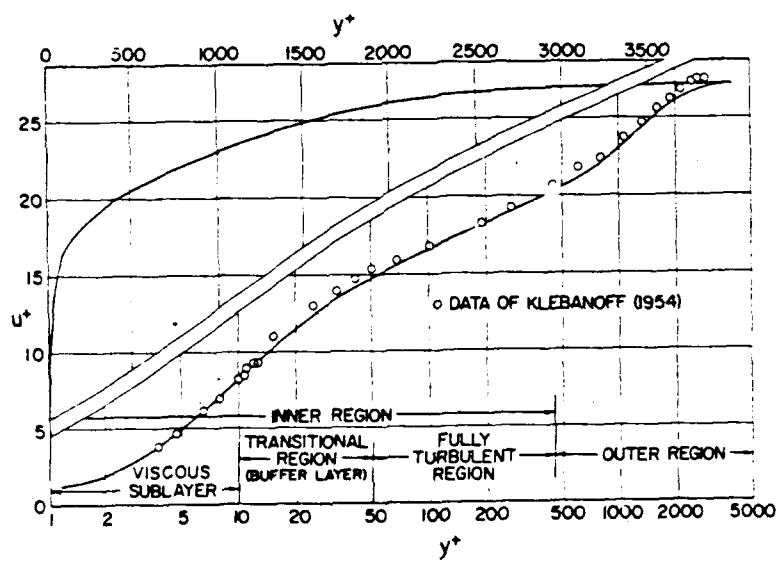

Figure 2. Semilog and Linear Plots of Mean Velocity Distribution Across a Turbulent Boundary Layer with Zero Pressure Gradient (5:94)

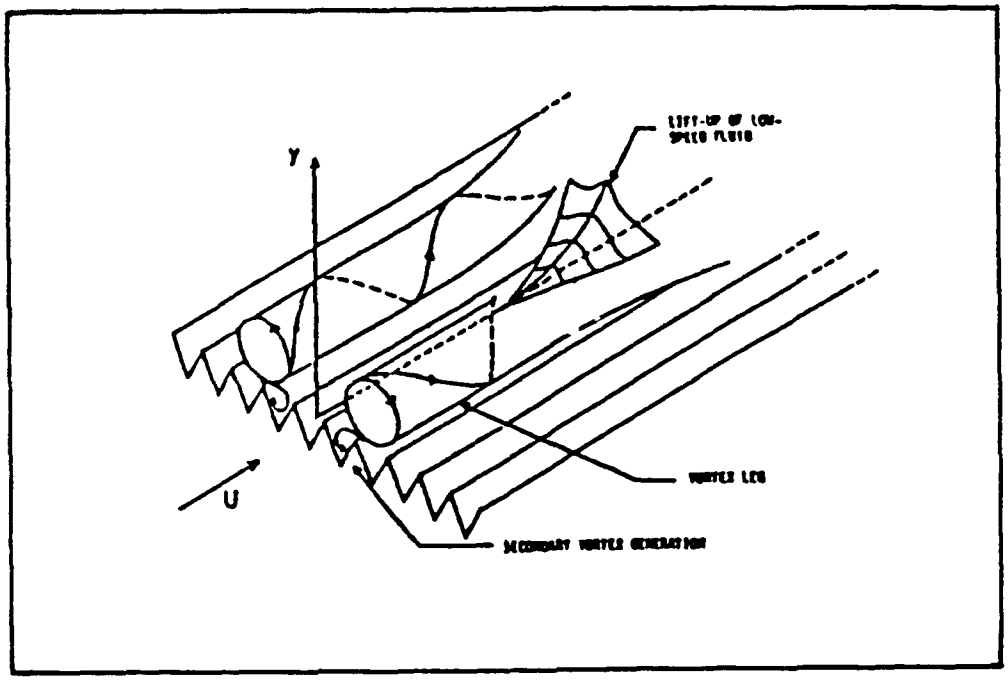

Figure 3. Secondary Vortex Generation on a Riblet Surface (2:1384)

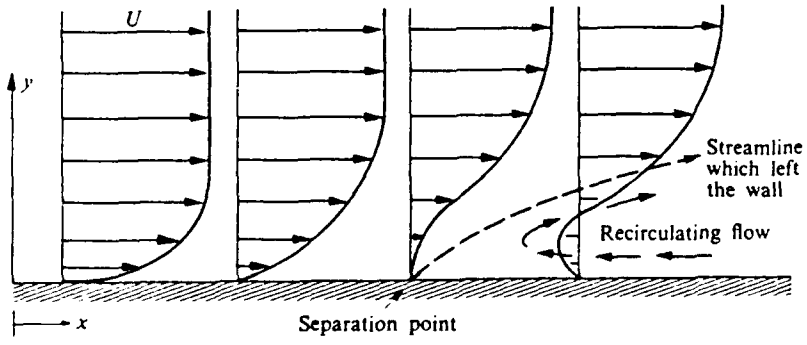

Figure 4. A Simplified Picture of the Development of Separation (8:68)

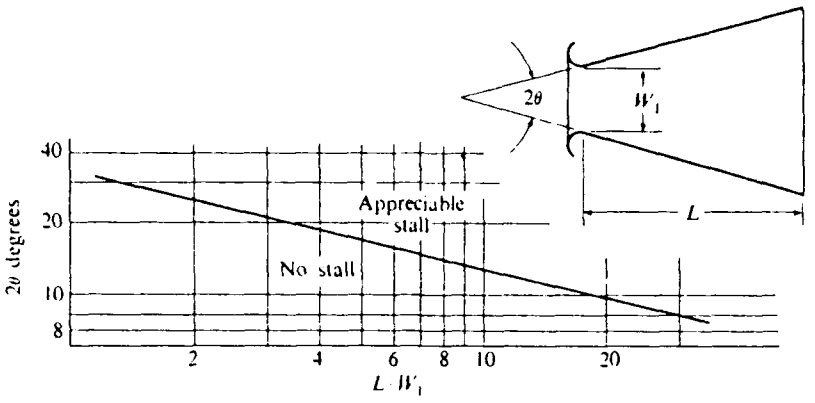

Figure 5. Stall Limits in Two-Dimensional Straight-Walled Diffusers (8:193)

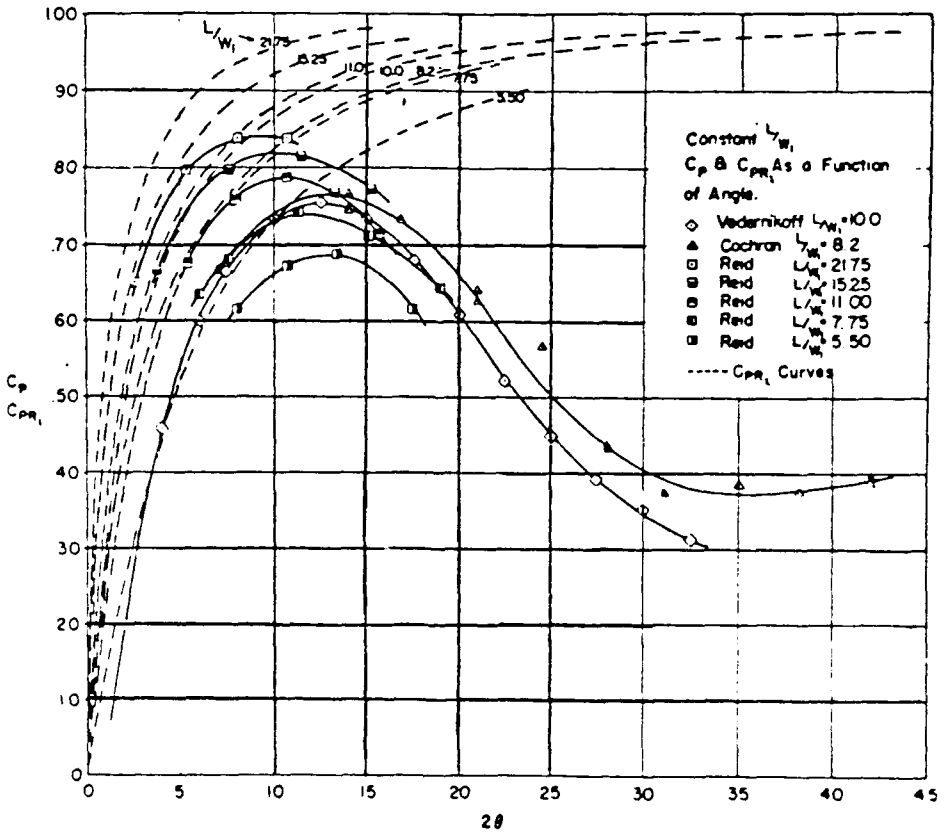

Figure 6. Two-Dimensional Diffuser Performance (15:394)

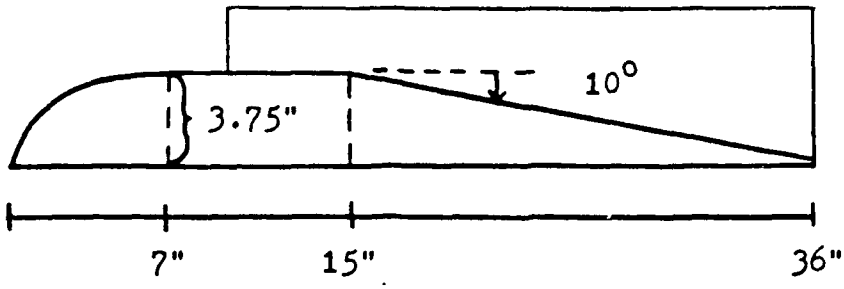

Figure 7. Side View of Diffuser Model with Vanes

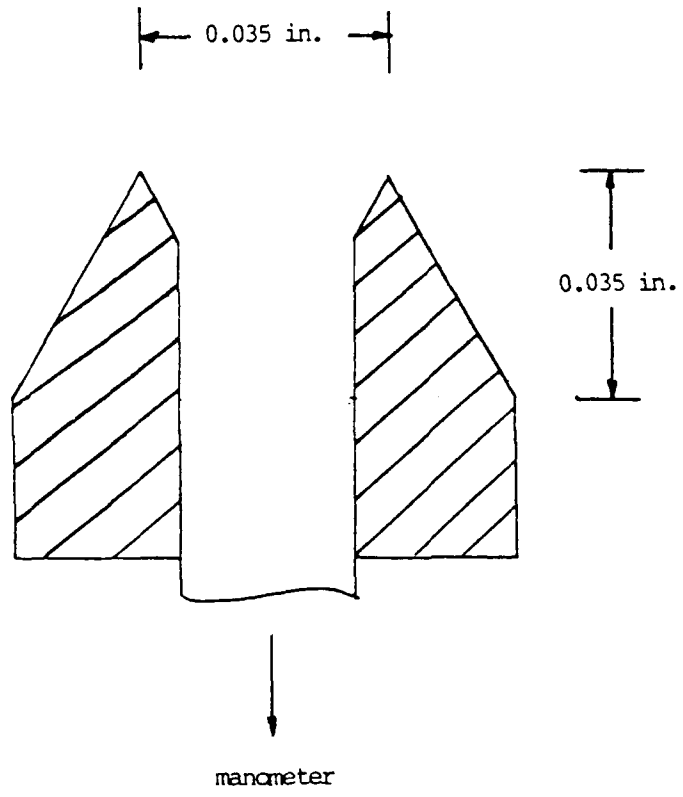

Figure 8. Static Port Location on Riblet Surface Ramp

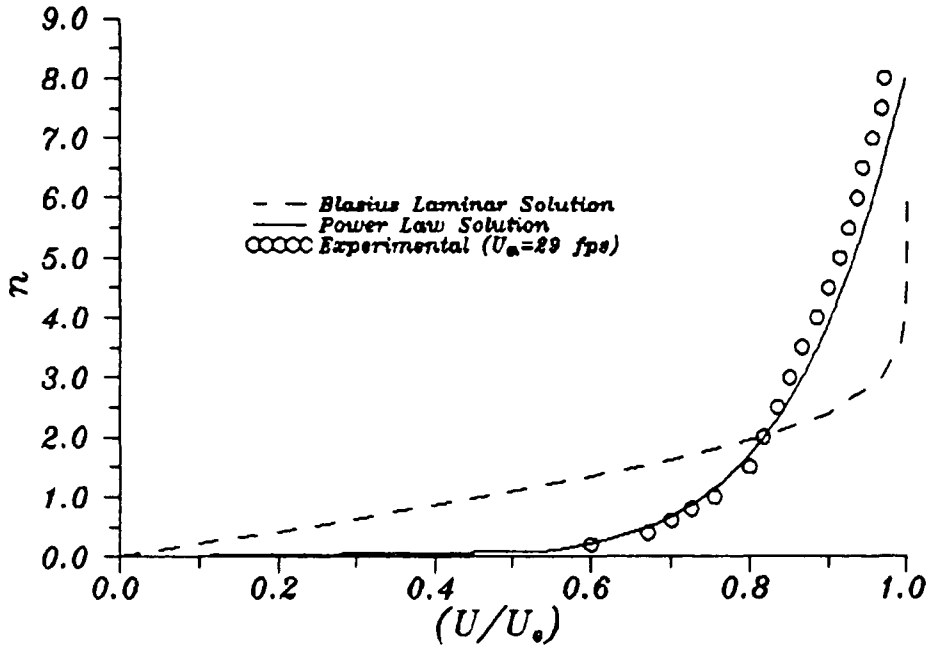

Figure 9. Experimental Turbulent and Theoretical Laminar Boundary Layer Profiles (Diffuser Throat U_{th} = 29 ft/sec) (16:313)

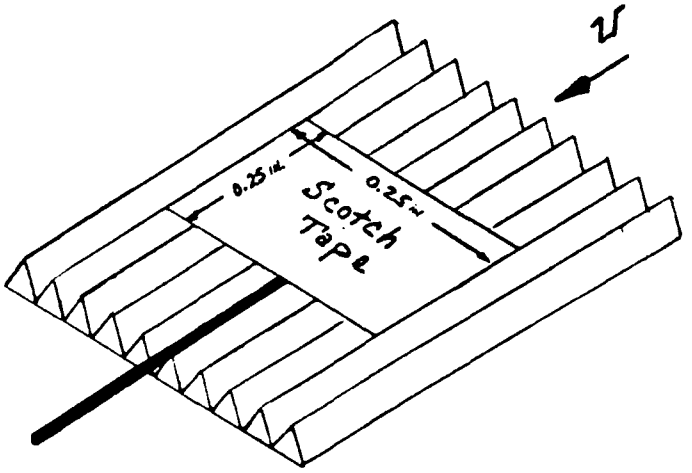

Figure 10. Tuft Attachment--Riblet Surface

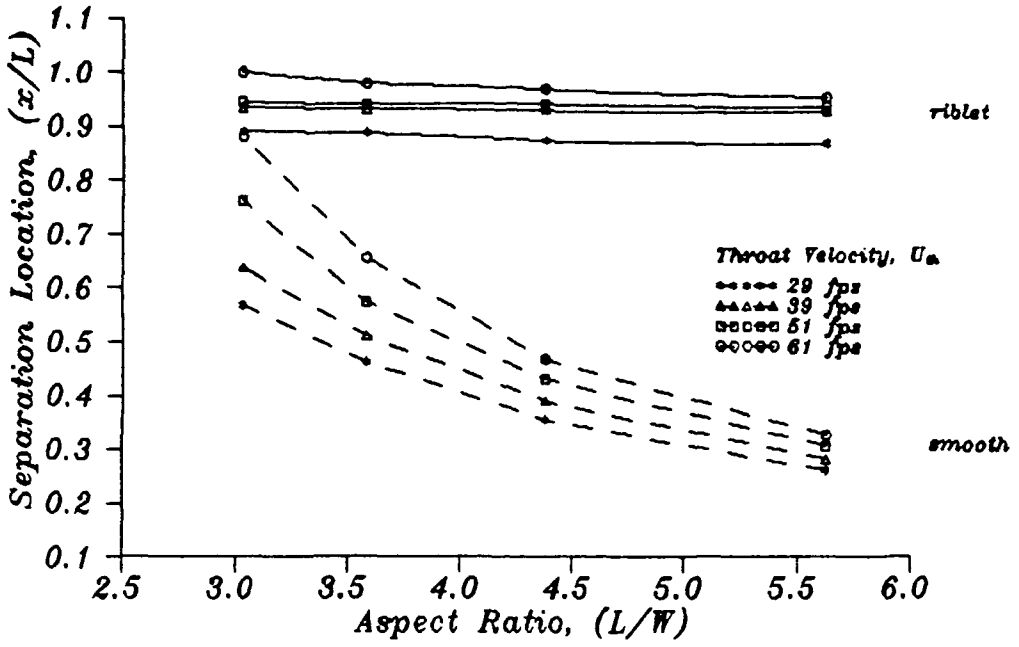

Figure 11. Separation Location vs. Aspect Ratio

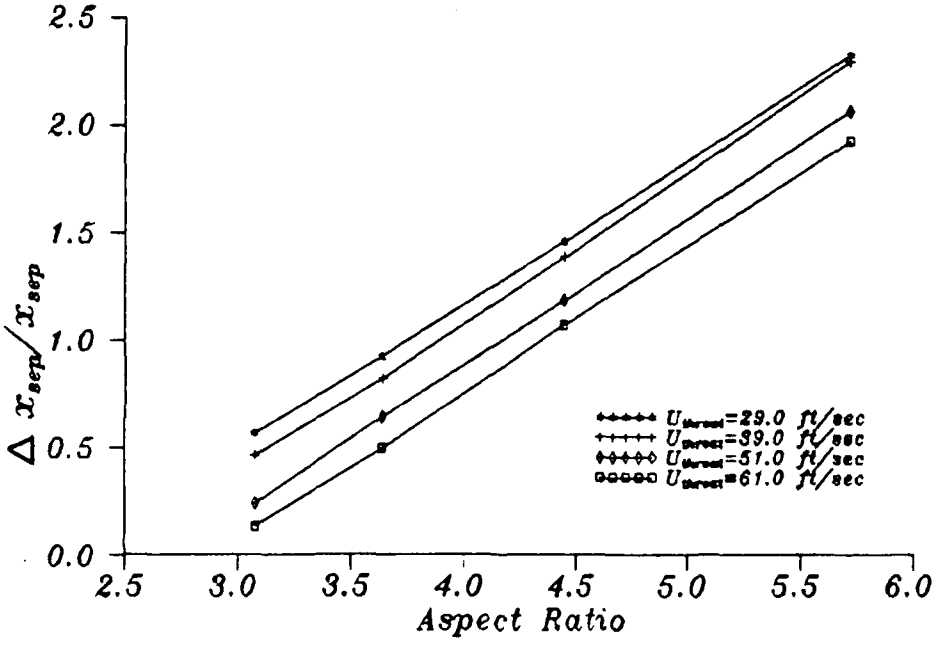

Figure 12. Attachment Enhancement vs. Aspect Ratio

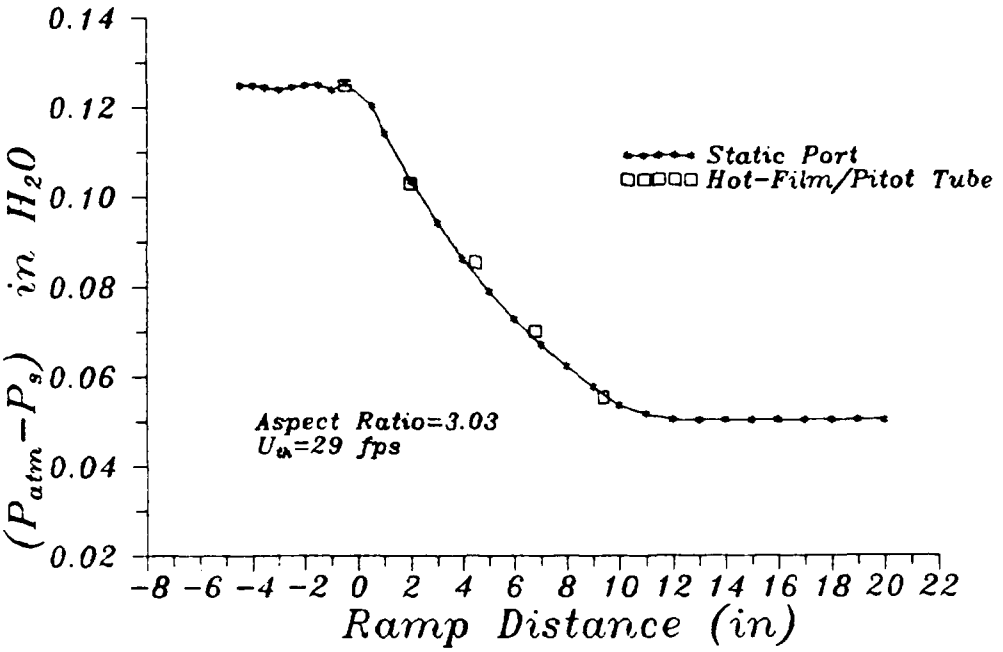

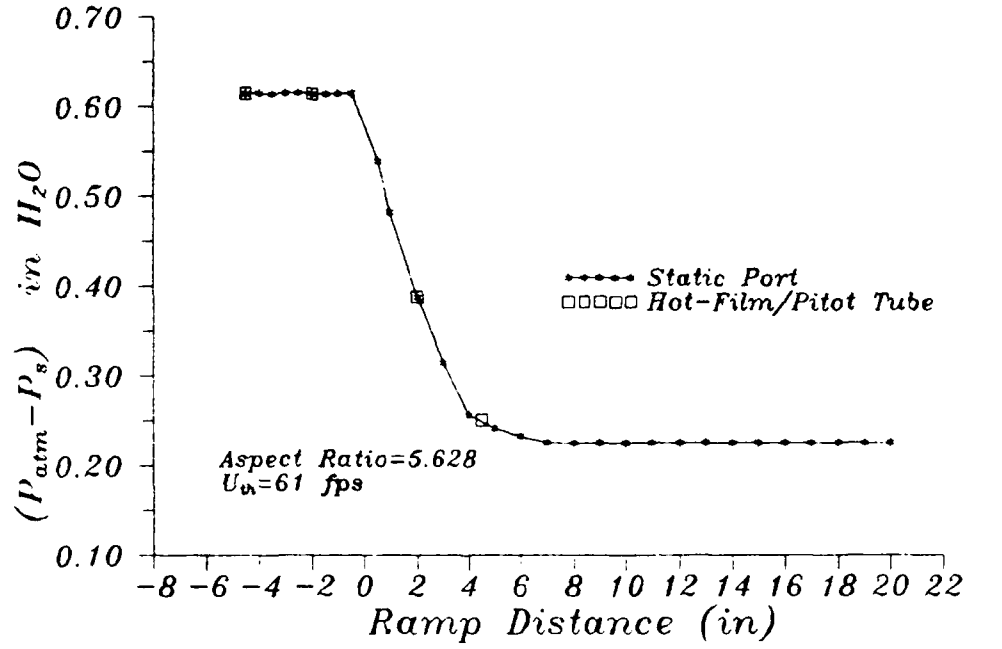

Figure 13. Comparison of Manometer and Anemometer/Pitot Tube-Derived Pressures

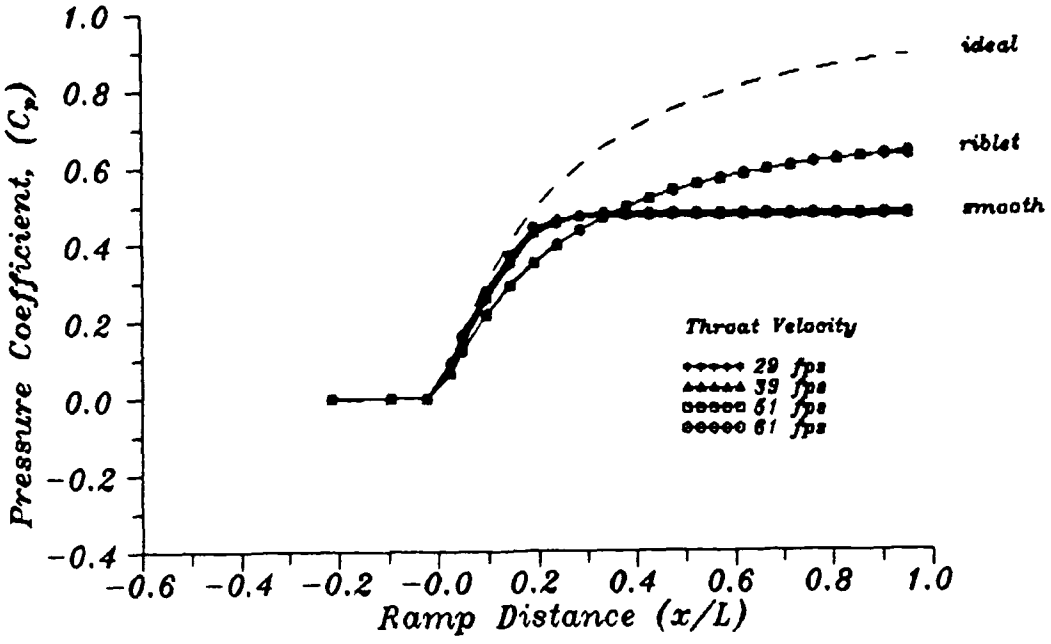

Figure 14. Pressure Coefficient vs. Ramp Distance (L/W)=5.628

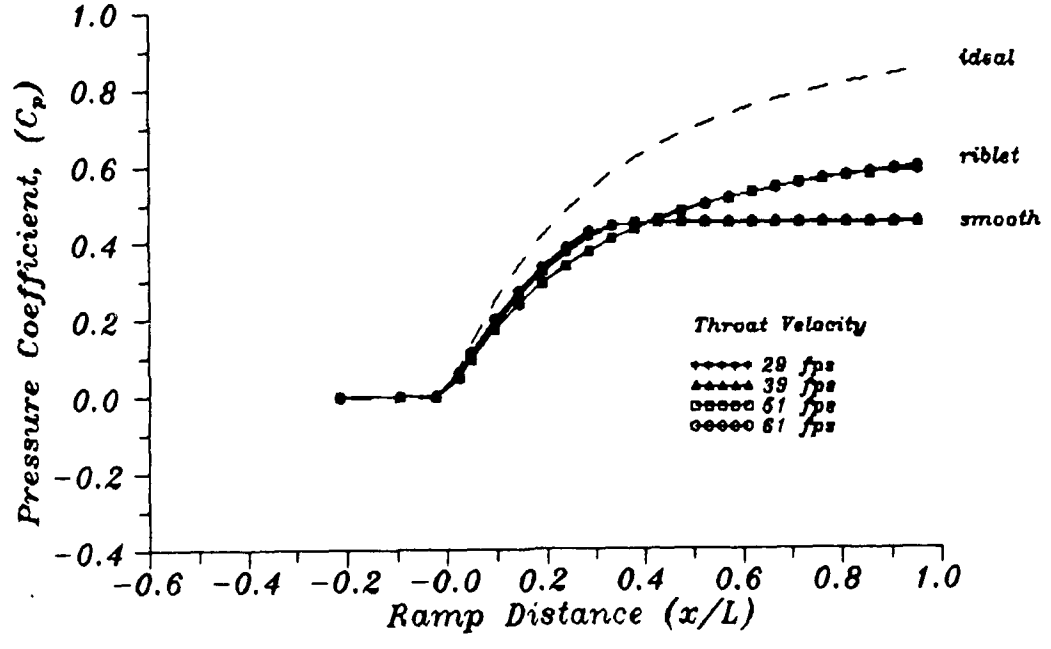

Figure 15. Pressure Coefficient vs. Ramp Distance (L/W)=4.377

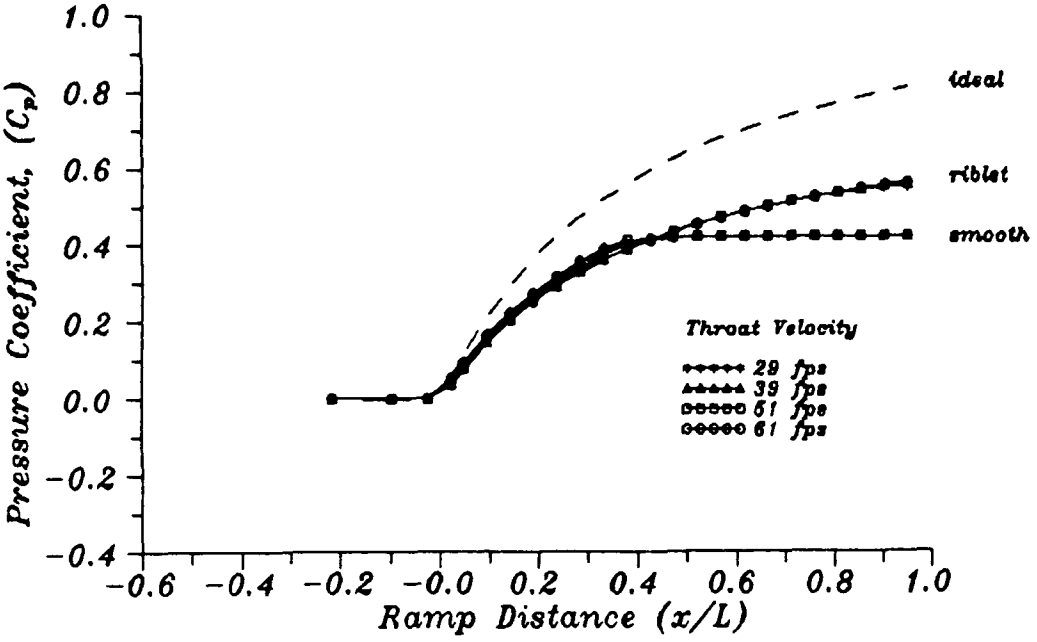

Figure 16. Pressure Coefficient vs. Ramp Distance (L/W)=3.581

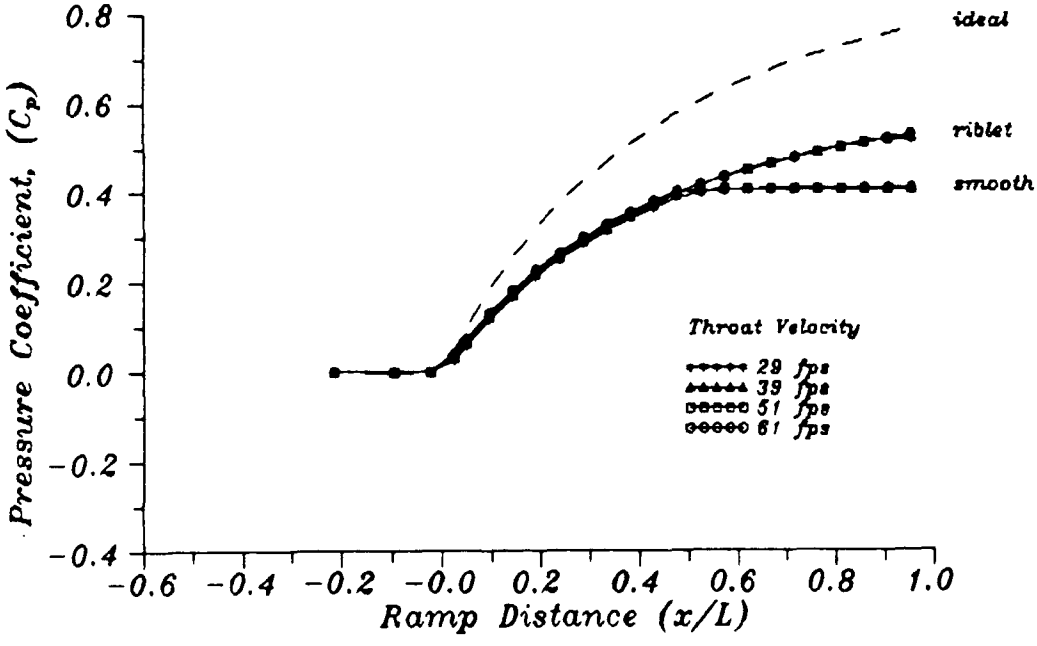

Figure 17. Pressure Coefficient vs. Ramp Distance (L/W)=3.030

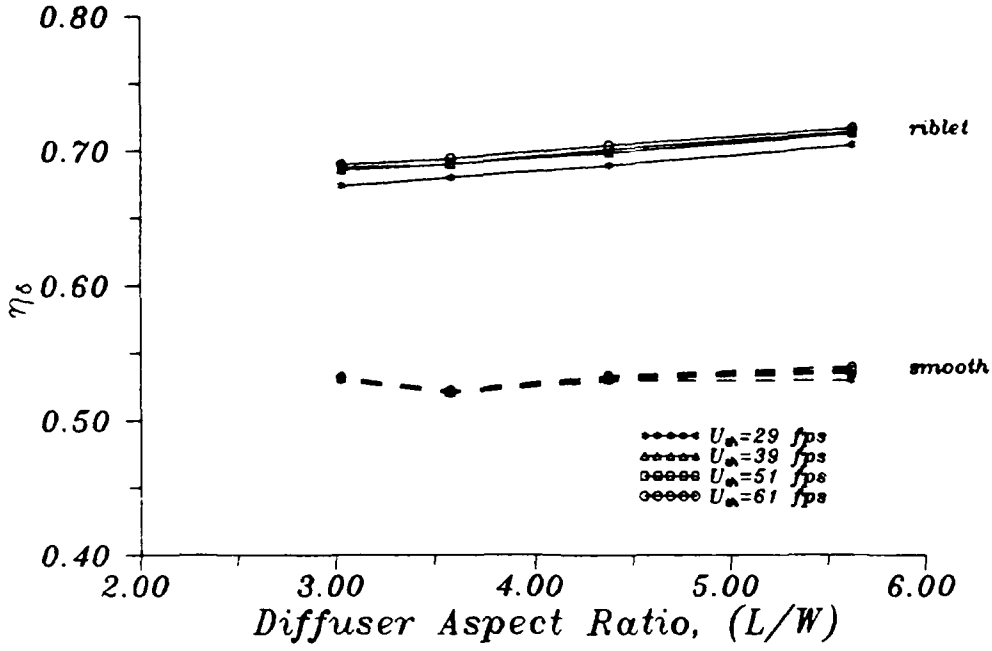

Figure 18. Diffuser Efficiency vs. Aspect Ratio

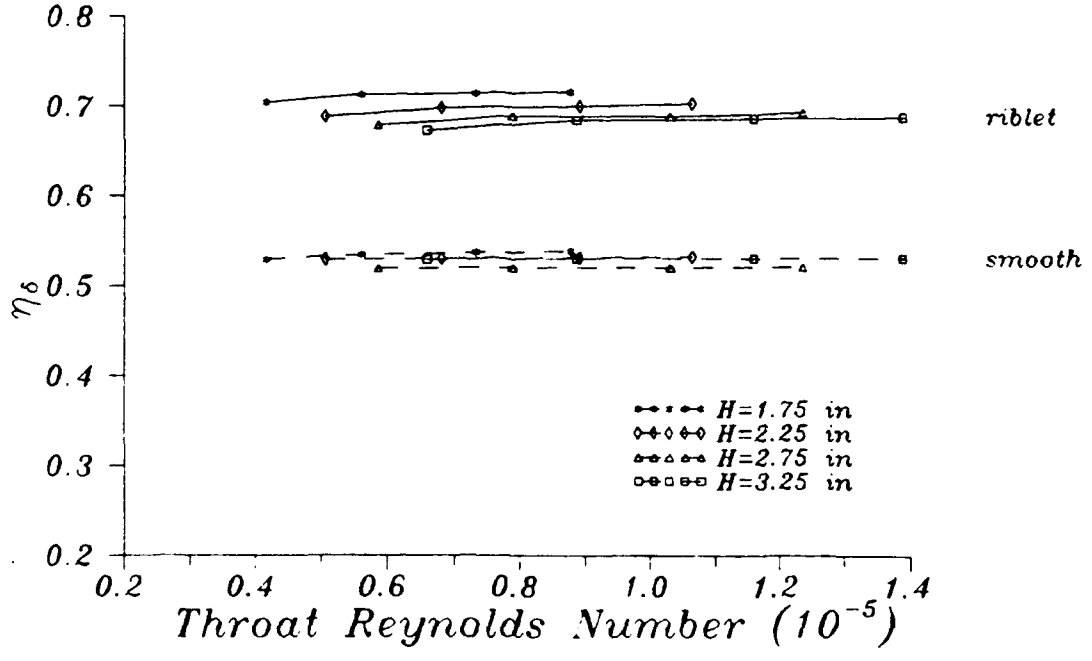

Figure 19. Diffuser Efficiency vs. Throat Reynolds Number

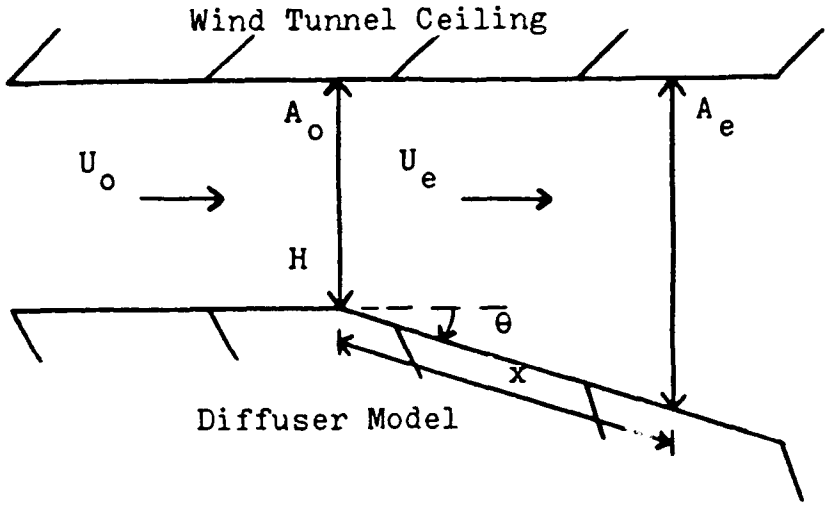

Figure 20. Side View of Test Diffuser Section

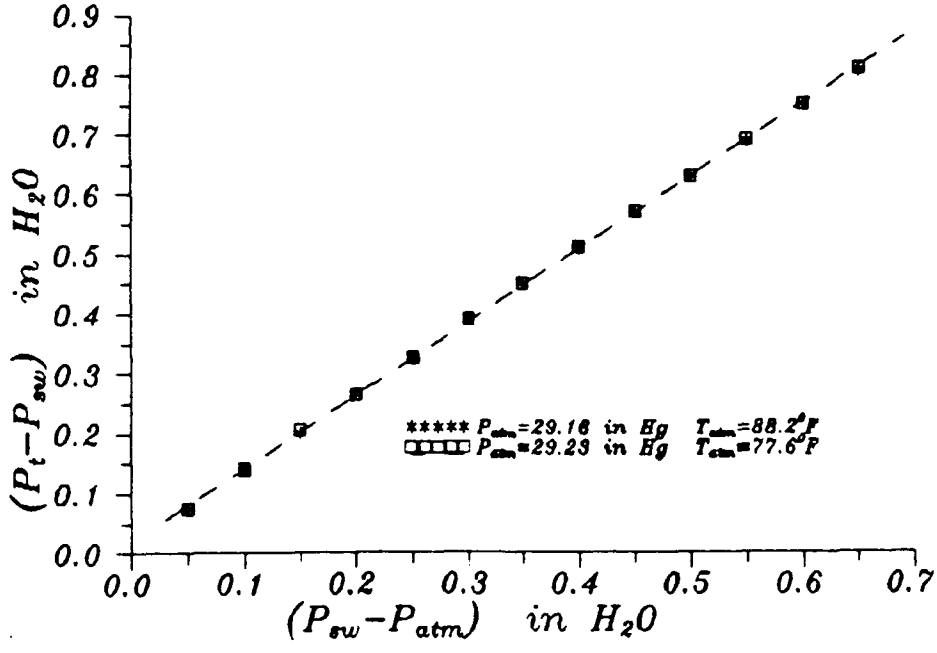

Figure 21. AFIT 9-Inch Wind Tunnel Calibration

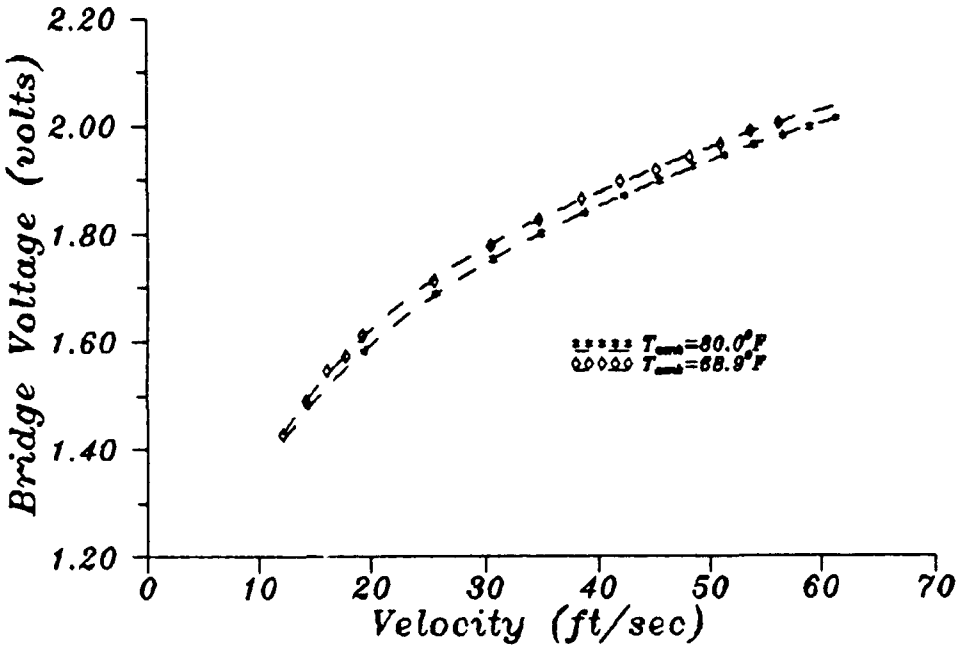

Figure 22. Hot-Film Calibration Curves for 68.9° F and 80.0° F

Appendix E Data

X	$(P_{stn}-P_s)_{smooth}$	$(C_p)_{smooth}$	$(P_{stn}-P_s)_{riblet}$	$(C_p)_{riblet}$
H= 1.75 in		U= 29 ft/sec		
P= 397.34 in H2O		T= 529.6701 R		
-4.5000	0.1254	-0.0020	0.1250	0.0000
-2.0000	0.1250	0.0003	0.1250	0.0000
-0.5000	0.1251	-0.0004	0.1250	0.0000
0.5000	0.1123	0.0689	0.1132	0.0642
1.0000	0.0994	0.1394	0.1022	0.1243
2.0000	0.0781	0.2554	0.0849	0.2183
3.0000	0.0615	0.3456	0.0714	0.2917
4.0000	0.0472	0.4234	0.0607	0.3501
5.0000	0.0422	0.4504	0.0521	0.3969
6.0000	0.0386	0.4704	0.0450	0.4352
7.0000	0.0386	0.4704	0.0391	0.4673
8.0000	0.0386	0.4704	0.0342	0.4939
9.0000	0.0386	0.4704	0.0300	0.5169
10.0000	0.0386	0.4704	0.0265	0.5363
11.0000	0.0386	0.4704	0.0233	0.5535
12.0000	0.0386	0.4704	0.0207	0.5677
13.0000	0.0386	0.4704	0.0184	0.5803
14.0000	0.0386	0.4704	0.0163	0.5914
15.0000	0.0386	0.4704	0.0145	0.6012
16.0000	0.0386	0.4704	0.0130	0.6097
17.0000	0.0386	0.4704	0.0115	0.6176
18.0000	0.0386	0.4704	0.0103	0.6244
19.0000	0.0386	0.4704	0.0100	0.6258
20.0000	0.0386	0.4704	0.0100	0.6258
H= 1.75 in		U= 39 ft/sec		
P= 397.34 in H2O		T= 529.6701 R		
-4.5000	0.2354	-0.0011	0.2350	0.0000
-2.0000	0.2351	-0.0002	0.2350	0.0000
-0.5000	0.2349	0.0004	0.2350	0.0000
0.5000	0.2102	0.0748	0.2134	0.0649
1.0000	0.1867	0.1453	0.1940	0.1235
2.0000	0.1482	0.2612	0.1627	0.2177
3.0000	0.1182	0.3515	0.1382	0.2913
4.0000	0.0924	0.4292	0.1188	0.3498
5.0000	0.0838	0.4550	0.1033	0.3965
6.0000	0.0771	0.4752	0.0904	0.4353
7.0000	0.0771	0.4752	0.0797	0.4676
8.0000	0.0771	0.4752	0.0708	0.4942
9.0000	0.0771	0.4752	0.0632	0.5172
10.0000	0.0771	0.4752	0.0568	0.5364
11.0000	0.0771	0.4752	0.0512	0.5534
12.0000	0.0771	0.4752	0.0464	0.5679
13.0000	0.0771	0.4752	0.0422	0.5804
14.0000	0.0771	0.4752	0.0385	0.5915
15.0000	0.0771	0.4752	0.0352	0.6013
16.0000	0.0771	0.4752	0.0323	0.6101
17.0000	0.0771	0.4752	0.0297	0.6179
18.0000	0.0771	0.4752	0.0275	0.6246
19.0000	0.0771	0.4752	0.0254	0.6310
20.0000	0.0771	0.4752	0.0245	0.6337

X	$(P_{atm}-P_s)_{smooth}$	$(C_p)_{smooth}$	$(P_{atm}-P_s)_{riblet}$	$(C_p)_{riblet}$
H= 1.75 in		U= 51 ft/sec		
P= 397.34 in H20		T= 529.6701 R		
-4.5000	0.4258	0.0000	0.4258	0.0000
-2.0000	0.4258	0.0000	0.4258	0.0000
-0.5000	0.4249	0.0001	0.4258	0.0000
0.5000	0.3754	0.0874	0.3878	0.0656
1.0000	0.3353	0.1579	0.3548	0.1237
2.0000	0.2695	0.2738	0.3013	0.2179
3.0000	0.2183	0.3641	0.2596	0.2913
4.0000	0.1779	0.4351	0.2264	0.3498
5.0000	0.1658	0.4565	0.1999	0.3964
6.0000	0.1587	0.4689	0.1779	0.4352
7.0000	0.1542	0.4769	0.1594	0.4677
8.0000	0.1542	0.4769	0.1443	0.4943
9.0000	0.1542	0.4769	0.1313	0.5172
10.0000	0.1542	0.4769	0.1203	0.5366
11.0000	0.1542	0.4769	0.1108	0.5534
12.0000	0.1542	0.4769	0.1026	0.5679
13.0000	0.1542	0.4769	0.0953	0.5806
14.0000	0.1542	0.4769	0.0891	0.5916
15.0000	0.1542	0.4769	0.0835	0.6015
16.0000	0.1542	0.4769	0.0785	0.6102
17.0000	0.1542	0.4769	0.0741	0.6180
18.0000	0.1542	0.4769	0.0703	0.6247
19.0000	0.1542	0.4769	0.0666	0.6311
20.0000	0.1542	0.4769	0.0646	0.6347
H= 1.75 in		U= 61 ft/sec		
P= 397.34 in H20		T= 529.6701 R		
-4.5000	0.6158	0.0000	0.6158	0.0000
-2.0000	0.6158	0.0000	0.6158	0.0000
-0.5000	0.6151	-0.0002	0.6158	0.0000
0.5000	0.5400	0.0924	0.5612	0.0663
1.0000	0.4824	0.1633	0.5146	0.1237
2.0000	0.3879	0.2797	0.4361	0.2179
3.0000	0.3149	0.3696	0.3785	0.2913
4.0000	0.2572	0.4407	0.3310	0.3498
5.0000	0.2417	0.4597	0.2927	0.3969
6.0000	0.2330	0.4705	0.2614	0.4355
7.0000	0.2259	0.4792	0.2354	0.4676
8.0000	0.2259	0.4792	0.2136	0.4943
9.0000	0.2259	0.4792	0.1951	0.5172
10.0000	0.2259	0.4792	0.1793	0.5366
11.0000	0.2259	0.4792	0.1657	0.5534
12.0000	0.2259	0.4792	0.1539	0.5679
13.0000	0.2259	0.4792	0.1436	0.5806
14.0000	0.2259	0.4792	0.1346	0.5916
15.0000	0.2259	0.4792	0.1268	0.6013
16.0000	0.2259	0.4792	0.1197	0.6101
17.0000	0.2259	0.4792	0.1132	0.6180
18.0000	0.2259	0.4792	0.1076	0.6250
19.0000	0.2259	0.4792	0.1026	0.6311
20.0000	0.2259	0.4792	0.0979	0.6369

X	$(P_{stn}-P_s)_{smooth}$	$(C_p)_{smooth}$	$(P_{stn}-P_s)_{riblet}$	$(C_p)_{riblet}$
H= 2.25 in		U= 29 ft/sec		
P= 397.34 in H2O		T= 529.6701 R		
-4.5000	0.1250	0.0000	0.1250	0.0000
-2.0000	0.1250	0.0000	0.1250	0.0000
-0.5000	0.1250	0.0000	0.1250	0.0000
0.5000	0.1165	0.0464	0.1156	0.0509
1.0000	0.1070	0.0960	0.1071	0.0973
2.0000	0.0908	0.1862	0.0927	0.1758
3.0000	0.0775	0.2583	0.0810	0.2396
4.0000	0.0665	0.3182	0.0712	0.2929
5.0000	0.0573	0.3683	0.0630	0.3375
6.0000	0.0496	0.4105	0.0561	0.3752
7.0000	0.0444	0.4389	0.0502	0.4074
8.0000	0.0427	0.4479	0.0451	0.4348
9.0000	0.0427	0.4479	0.0407	0.4590
10.0000	0.0427	0.4479	0.0370	0.4791
11.0000	0.0427	0.4479	0.0337	0.4971
12.0000	0.0427	0.4479	0.0307	0.5132
13.0000	0.0427	0.4479	0.0279	0.5286
14.0000	0.0427	0.4479	0.0257	0.5407
15.0000	0.0427	0.4479	0.0236	0.5521
16.0000	0.0427	0.4479	0.0216	0.5628
17.0000	0.0427	0.4479	0.0200	0.5715
18.0000	0.0427	0.4479	0.0184	0.5802
19.0000	0.0427	0.4479	0.0179	0.5829
20.0000	0.0427	0.4479	0.0179	0.5829
H= 2.25 in		U= 39 ft/sec		
P= 397.34 in H2O		T= 529.6701 R		
-4.5000	0.2350	0.0000	0.2350	0.0000
-2.0000	0.2350	0.0000	0.2350	0.0000
-0.5000	0.2351	-0.0003	0.2350	0.0000
0.5000	0.2176	0.0525	0.2180	0.0511
1.0000	0.2007	0.1033	0.2027	0.0972
2.0000	0.1714	0.1915	0.1765	0.1759
3.0000	0.1474	0.2636	0.1554	0.2396
4.0000	0.1275	0.3235	0.1376	0.2931
5.0000	0.1109	0.3735	0.1230	0.3371
6.0000	0.0969	0.4158	0.1104	0.3751
7.0000	0.0890	0.4395	0.0998	0.4071
8.0000	0.0860	0.4485	0.0906	0.4346
9.0000	0.0858	0.4490	0.0828	0.4583
10.0000	0.0858	0.4490	0.0757	0.4795
11.0000	0.0858	0.4490	0.0696	0.4978
12.0000	0.0858	0.4490	0.0643	0.5139
13.0000	0.0858	0.4490	0.0593	0.5288
14.0000	0.0858	0.4490	0.0552	0.5412
15.0000	0.0858	0.4490	0.0515	0.5524
16.0000	0.0858	0.4490	0.0483	0.5621
17.0000	0.0858	0.4490	0.0450	0.5720
18.0000	0.0858	0.4490	0.0437	0.5758
19.0000	0.0858	0.4490	0.0398	0.5876
20.0000	0.0858	0.4490	0.0387	0.5909

X	$(P_{stn}-P_s)_{smooth}$	$(C_p)_{smooth}$	$(P_{stn}-P_s)_{riblet}$	$(C_p)_{riblet}$
H= 2.25 in		U= 51 ft/sec		
P= 397.34 in H2O		T= 529.6701 R		
-4.5000	0.4250	0.0000	0.4250	0.0000
-2.0000	0.4250	0.0000	0.4250	0.0000
-0.5000	0.4255	-0.0009	0.4250	0.0000
0.5000	0.3922	0.0578	0.3961	0.0509
1.0000	0.3633	0.1086	0.3698	0.0972
2.0000	0.3133	0.1968	0.3251	0.1759
3.0000	0.2726	0.2684	0.2886	0.2399
4.0000	0.2383	0.3287	0.2584	0.2933
5.0000	0.2096	0.3793	0.2333	0.3375
6.0000	0.1857	0.4215	0.2121	0.3749
7.0000	0.1752	0.4400	0.1938	0.4072
8.0000	0.1700	0.4490	0.1777	0.4355
9.0000	0.1694	0.4502	0.1642	0.4594
10.0000	0.1694	0.4502	0.1525	0.4799
11.0000	0.1694	0.4502	0.1421	0.4982
12.0000	0.1694	0.4502	0.1329	0.5144
13.0000	0.1694	0.4502	0.1248	0.5288
14.0000	0.1694	0.4502	0.1175	0.5415
15.0000	0.1694	0.4502	0.1111	0.5529
16.0000	0.1694	0.4502	0.1058	0.5621
17.0000	0.1694	0.4502	0.1000	0.5723
18.0000	0.1694	0.4502	0.0954	0.5805
19.0000	0.1694	0.4502	0.0910	0.5881
20.0000	0.1694	0.4502	0.0883	0.5930
H= 2.25 in		U= 61 ft/sec		
P= 397.34 in H2O		T= 529.6701 R		
-4.5000	0.6165	-0.0018	0.6150	0.0000
-2.0000	0.6150	0.0000	0.6150	0.0000
-0.5000	0.6144	0.0008	0.6150	0.0000
0.5000	0.5638	0.0630	0.5733	0.0513
1.0000	0.5226	0.1139	0.5358	0.0976
2.0000	0.4509	0.2021	0.4727	0.1753
3.0000	0.3928	0.2737	0.4200	0.2401
4.0000	0.3440	0.3337	0.3773	0.2928
5.0000	0.3028	0.3845	0.3408	0.3377
6.0000	0.2685	0.4268	0.3101	0.3755
7.0000	0.2569	0.4410	0.2841	0.4075
8.0000	0.2497	0.4499	0.2625	0.4342
9.0000	0.2492	0.4505	0.2430	0.4581
10.0000	0.2488	0.4510	0.2264	0.4787
11.0000	0.2488	0.4510	0.2113	0.4971
12.0000	0.2488	0.4510	0.1976	0.5140
13.0000	0.2488	0.4510	0.1857	0.5288
14.0000	0.2488	0.4510	0.1763	0.5403
15.0000	0.2488	0.4510	0.1668	0.5519
16.0000	0.2488	0.4510	0.1575	0.5635
17.0000	0.2488	0.4510	0.1503	0.5723
18.0000	0.2488	0.4510	0.1435	0.5808
19.0000	0.2488	0.4510	0.1371	0.5885
20.0000	0.2488	0.4510	0.1314	0.5956

X	$(P_{atm}-P_s)_{smooth}$	$(C_p)_{smooth}$	$(P_{atm}-P_s)_{riblet}$	$(C_p)_{riblet}$
H= 2.75 in P= 396.58 in H2O		U= 29 ft/sec T= 528.6701 R		
-4.5000	0.1250	0.0000	0.1250	0.0000
-2.0000	0.1253	-0.0017	0.1250	0.0000
-0.5000	0.1251	-0.0004	0.1250	0.0000
0.5000	0.1189	0.0334	0.1173	0.0416
1.0000	0.1115	0.0735	0.1103	0.0800
2.0000	0.0986	0.1436	0.0988	0.1469
3.0000	0.0877	0.2029	0.0877	0.2029
4.0000	0.0784	0.2535	0.0787	0.2523
5.0000	0.0705	0.2969	0.0713	0.2924
6.0000	0.0634	0.3353	0.0649	0.3274
7.0000	0.0569	0.3708	0.0588	0.3604
8.0000	0.0509	0.4033	0.0537	0.3882
9.0000	0.0496	0.4102	0.0494	0.4116
10.0000	0.0481	0.4186	0.0454	0.4334
11.0000	0.0481	0.4186	0.0418	0.4527
12.0000	0.0481	0.4186	0.0387	0.4695
13.0000	0.0481	0.4186	0.0359	0.4847
14.0000	0.0481	0.4186	0.0334	0.4984
15.0000	0.0481	0.4186	0.0312	0.5106
16.0000	0.0481	0.4186	0.0290	0.5222
17.0000	0.0481	0.4186	0.0271	0.5328
18.0000	0.0481	0.4186	0.0255	0.5417
19.0000	0.0481	0.4186	0.0244	0.5474
20.0000	0.0481	0.4186	0.0244	0.5474
H= 2.75 in P= 396.58 in H2O		U= 39 ft/sec T= 528.6701 R		
-4.5000	0.2350	0.0000	0.2350	0.0000
-2.0000	0.2350	0.0000	0.2350	0.0000
-0.5000	0.2350	0.0000	0.2350	0.0000
0.5000	0.2223	0.0383	0.2211	0.0418
1.0000	0.2090	0.0783	0.2084	0.0801
2.0000	0.1857	0.1484	0.1861	0.1472
3.0000	0.1660	0.2078	0.1674	0.2036
4.0000	0.1492	0.2584	0.1513	0.2520
5.0000	0.1348	0.3017	0.1377	0.2928
6.0000	0.1220	0.3401	0.1260	0.3281
7.0000	0.1102	0.3756	0.1153	0.3603
8.0000	0.1003	0.4054	0.1061	0.3880
9.0000	0.0980	0.4123	0.0981	0.4121
10.0000	0.0959	0.4186	0.0909	0.4338
11.0000	0.0957	0.4193	0.0846	0.4526
12.0000	0.0957	0.4193	0.0790	0.4697
13.0000	0.0957	0.4193	0.0738	0.4852
14.0000	0.0957	0.4193	0.0693	0.4988
15.0000	0.0957	0.4193	0.0651	0.5115
16.0000	0.0957	0.4193	0.0613	0.5229
17.0000	0.0957	0.4193	0.0579	0.5331
18.0000	0.0957	0.4193	0.0548	0.5425
19.0000	0.0957	0.4193	0.0520	0.5508
20.0000	0.0957	0.4193	0.0505	0.5553

X	$(P_{stn}-P_s)_{smooth}$	$(C_p)_{smooth}$	$(P_{stn}-P_s)_{riblet}$	$(C_p)_{riblet}$
H= 2.75 in		U= 51 ft/sec		
P= 396.58 in H2O		T= 528.6701 R		
-4.5000	0.4250	0.0000	0.4250	0.0000
-2.0000	0.4250	0.0000	0.4250	0.0000
-0.5000	0.4250	0.0000	0.4250	0.0000
0.5000	0.3975	0.0485	0.4011	0.0420
1.0000	0.3746	0.0887	0.3794	0.0804
2.0000	0.3348	0.1588	0.3413	0.1474
3.0000	0.3014	0.2176	0.3092	0.2039
4.0000	0.2731	0.2675	0.2817	0.2524
5.0000	0.2479	0.3119	0.2582	0.2938
6.0000	0.2263	0.3500	0.2379	0.3295
7.0000	0.2078	0.3825	0.2206	0.3600
8.0000	0.1917	0.4109	0.2046	0.3862
9.0000	0.1896	0.4145	0.1908	0.4125
10.0000	0.1871	0.4190	0.1786	0.4339
11.0000	0.1868	0.4195	0.1681	0.4524
12.0000	0.1866	0.4198	0.1579	0.4704
13.0000	0.1866	0.4198	0.1494	0.4853
14.0000	0.1866	0.4198	0.1418	0.4987
15.0000	0.1866	0.4198	0.1348	0.5111
16.0000	0.1866	0.4198	0.1281	0.5229
17.0000	0.1866	0.4198	0.1228	0.5321
18.0000	0.1866	0.4198	0.1168	0.5427
19.0000	0.1866	0.4198	0.1126	0.5503
20.0000	0.1866	0.4198	0.1097	0.5553
H= 2.75 in		U= 61 ft/sec		
P= 396.58 in H2O		T= 528.6701 R		
-4.5000	0.6150	0.0000	0.6150	0.0000
-2.0000	0.6150	0.0000	0.6150	0.0000
-0.5000	0.6150	0.0000	0.6150	0.0000
0.5000	0.5717	0.0534	0.5812	0.0416
1.0000	0.5390	0.0936	0.5501	0.0800
2.0000	0.4822	0.1635	0.4957	0.1469
3.0000	0.4347	0.2220	0.4498	0.2035
4.0000	0.3943	0.2718	0.4106	0.2517
5.0000	0.3584	0.3160	0.3770	0.2931
6.0000	0.3269	0.3548	0.3477	0.3292
7.0000	0.2999	0.3881	0.3225	0.3603
8.0000	0.2809	0.4115	0.3003	0.3876
9.0000	0.2793	0.4135	0.2809	0.4114
10.0000	0.2746	0.4193	0.2633	0.4331
11.0000	0.2741	0.4199	0.2479	0.4522
12.0000	0.2738	0.4202	0.2339	0.4693
13.0000	0.2738	0.4202	0.2213	0.4849
14.0000	0.2738	0.4202	0.2103	0.4984
15.0000	0.2738	0.4202	0.1996	0.5117
16.0000	0.2738	0.4202	0.1910	0.5222
17.0000	0.2738	0.4202	0.1824	0.5328
18.0000	0.2738	0.4202	0.1746	0.5425
19.0000	0.2738	0.4202	0.1677	0.5509
20.0000	0.2738	0.4202	0.1614	0.5587

X	$(P_{atm}-P_s)_{smooth}$	$(C_p)_{smooth}$	$(P_{atm}-P_s)_{riblet}$	$(C_p)_{riblet}$
H= 3.25 in P= 396.58 in H2O		U= 29 ft/sec T= 528.6701 R		
-4.5000	0.1250	0.0000	0.1250	0.0000
-2.0000	0.1250	0.0000	0.1250	0.0000
-0.5000	0.1250	0.0000	0.1250	0.0000
0.5000	0.1203	0.0256	0.1185	0.0352
1.0000	0.1143	0.0581	0.1126	0.0677
2.0000	0.1035	0.1169	0.1017	0.1268
3.0000	0.0943	0.1670	0.0925	0.1771
4.0000	0.0862	0.2114	0.0842	0.2221
5.0000	0.0791	0.2501	0.0773	0.2595
6.0000	0.0728	0.2842	0.0708	0.2950
7.0000	0.0672	0.3147	0.0653	0.3248
8.0000	0.0623	0.3411	0.0604	0.3515
9.0000	0.0578	0.3656	0.0559	0.3761
10.0000	0.0536	0.3885	0.0520	0.3971
11.0000	0.0517	0.3990	0.0485	0.4163
12.0000	0.0504	0.4060	0.0452	0.4344
13.0000	0.0504	0.4060	0.0422	0.4504
14.0000	0.0504	0.4060	0.0398	0.4638
15.0000	0.0504	0.4060	0.0372	0.4776
16.0000	0.0504	0.4060	0.0349	0.4901
17.0000	0.0504	0.4060	0.0330	0.5009
18.0000	0.0504	0.4060	0.0311	0.5113
19.0000	0.0504	0.4060	0.0301	0.5164
20.0000	0.0504	0.4060	0.0301	0.5164
H= 3.25 in P= 396.58 in H2O		U= 39 ft/sec T= 528.6701 R		
-4.5000	0.2350	0.0000	0.2350	0.0000
-2.0000	0.2353	-0.0011	0.2350	0.0000
-0.5000	0.2350	0.0000	0.2350	0.0000
0.5000	0.2249	0.0304	0.2232	0.0356
1.0000	0.2143	0.0624	0.2123	0.0663
2.0000	0.1947	0.1213	0.1927	0.1275
3.0000	0.1781	0.1713	0.1762	0.1771
4.0000	0.1631	0.2163	0.1612	0.2221
5.0000	0.1505	0.2544	0.1484	0.2606
6.0000	0.1391	0.2887	0.1370	0.2950
7.0000	0.1290	0.3192	0.1270	0.3252
8.0000	0.1202	0.3455	0.1181	0.3519
9.0000	0.1121	0.3699	0.1102	0.3758
10.0000	0.1019	0.4006	0.1030	0.3975
11.0000	0.1012	0.4027	0.0968	0.4161
12.0000	0.1003	0.4055	0.0906	0.4348
13.0000	0.1000	0.4064	0.0853	0.4506
14.0000	0.0997	0.4072	0.0806	0.4649
15.0000	0.0997	0.4072	0.0765	0.4770
16.0000	0.0997	0.4072	0.0722	0.4900
17.0000	0.0997	0.4072	0.0686	0.5010
18.0000	0.0997	0.4072	0.0652	0.5111
19.0000	0.0997	0.4072	0.0620	0.5207
20.0000	0.0997	0.4072	0.0604	0.5256

X	$(P_{atm}-P_s)_{smooth}$	$(C_p)_{smooth}$	$(P_{atm}-P_s)_{riblet}$	$(C_p)_{riblet}$
H= 3.25 in P= 396.58 in H20			U= 51 ft/sec T= 528.6701 R	
-4.5000	0.4250	0.0000	0.4250	0.0000
-2.0000	0.4250	0.0000	0.4250	0.0000
-0.5000	0.4250	0.0000	0.4250	0.0000
0.5000	0.4049	0.0355	0.4046	0.0359
1.0000	0.3866	0.0677	0.3865	0.0678
2.0000	0.3529	0.1269	0.3532	0.1264
3.0000	0.3244	0.1773	0.3248	0.1765
4.0000	0.3016	0.2173	0.2997	0.2208
5.0000	0.2800	0.2554	0.2776	0.2596
6.0000	0.2608	0.2892	0.2582	0.2938
7.0000	0.2434	0.3198	0.2411	0.3239
8.0000	0.2288	0.3455	0.2258	0.3508
9.0000	0.2142	0.3712	0.2124	0.3745
10.0000	0.1972	0.4012	0.1997	0.3968
11.0000	0.1965	0.4025	0.1892	0.4152
12.0000	0.1945	0.4059	0.1788	0.4336
13.0000	0.1942	0.4065	0.1698	0.4494
14.0000	0.1937	0.4074	0.1616	0.4638
15.0000	0.1937	0.4073	0.1543	0.4767
16.0000	0.1936	0.4075	0.1474	0.4888
17.0000	0.1936	0.4075	0.1407	0.5006
18.0000	0.1936	0.4075	0.1355	0.5098
19.0000	0.1936	0.4075	0.1303	0.5190
20.0000	0.1936	0.4075	0.1258	0.5269
H= 3.25 in P= 396.58 in H20			U= 61 ft/sec T= 528.6701 R	
-4.5000	0.6150	0.0000	0.6150	0.0000
-2.0000	0.6150	0.0000	0.6150	0.0000
-0.5000	0.6150	0.0000	0.6150	0.0000
0.5000	0.5825	0.0401	0.5862	0.0355
1.0000	0.5563	0.0723	0.5596	0.0682
2.0000	0.5082	0.1315	0.5120	0.1268
3.0000	0.4676	0.1816	0.4710	0.1774
4.0000	0.4317	0.2257	0.4351	0.2215
5.0000	0.4003	0.2644	0.4038	0.2602
6.0000	0.3724	0.2988	0.3760	0.2943
7.0000	0.3482	0.3286	0.3516	0.3244
8.0000	0.3264	0.3554	0.3298	0.3512
9.0000	0.3065	0.3800	0.3103	0.3753
10.0000	0.2895	0.4009	0.2928	0.3968
11.0000	0.2864	0.4022	0.2771	0.4161
12.0000	0.2858	0.4055	0.2628	0.4338
13.0000	0.2849	0.4066	0.2499	0.4497
14.0000	0.2844	0.4072	0.2382	0.4641
15.0000	0.2843	0.4073	0.2275	0.4772
16.0000	0.2841	0.4075	0.2177	0.4893
17.0000	0.2841	0.4076	0.2087	0.5004
18.0000	0.2839	0.4078	0.2004	0.5106
19.0000	0.2838	0.4079	0.1928	0.5199
20.0000	0.2838	0.4079	0.1858	0.5286

Vita

Captain Michael K. Reagan was born on 20 August 1959 in Palo Alto, California. He graduated from Saint Francis High School, Mountain View, California, in 1977 and attended the United States Air Force Academy, where he earned the degree of Bachelor of Science in Aeronautical Engineering. Upon graduation in 1981, he was assigned to Undergraduate Pilot Training at Reese AFB, where he graduated in 1982. He remained as a T-37 instructor pilot until 1985, when he was reassigned to Randolph AFB and the Pilot Instructor Training Center. In 1987, he was reassigned to Luke AFB as a student pilot in the F-15 Replacement Training Unit with a follow-on assignment to Keflavik NAS, Iceland. A medical disqualification removed him from the program and reassigned him to Randolph AFB as the executive officer to the Wing Commander, until entering the School of Engineering, Air Force Institute of Technology, in May of 1989.

Permanent Address: 3410 Pebblecreek Drive
Beavercreek, Ohio 45432

REPORT DOCUMENTATION PAGE

Form Approved
OMB No 0704-0188

1. AGENCY USE ONLY (Leave blank)	2. REPORT DATE	3. REPORT TYPE AND DATES COVERED
	December 1990	Master's Thesis

4. TITLE AND SUBTITLE
EFFECT OF RIBLETS ON PRESSURE RECOVERY IN A STRAIGHT-WALLED DIFFUSER

5. FUNDING NUMBERS

6. AUTHOR(S)
Michael K. Reagan, Captain, USAF

7. PERFORMING ORGANIZATION NAME(S) AND ADDRESS(ES)
AFIT/ENY
WPAFB OH 45433

8. PERFORMING ORGANIZATION REPORT NUMBER
AFIT/GAE/ENY/90D-21

9. SPONSORING/MONITORING AGENCY NAME(S) AND ADDRESS(ES)

10. SPONSORING/MONITORING AGENCY REPORT NUMBER

11. SUPPLEMENTARY NOTES

12a. DISTRIBUTION/AVAILABILITY STATEMENT
Approved for public release; distribution unlimited

12b. DISTRIBUTION CODE

13. ABSTRACT (Maximum 200 words)
The objective of this thesis was to investigate the effect of riblets on the pressure recovery in a straight-walled diffuser. Previous work has shown that riblets were effective in reducing the viscous drag over surfaces subjected to a turbulent boundary layer. More recently, riblets were shown to delay the flow separation within a subsonic, straight-walled diffuser by as much as 200 percent. The purpose of this investigation was to determine the effect on the pressure distribution within a diffuser that has had the flow separation point favorably altered by the application of riblets. Results from this investigation revealed that riblets not only delayed flow separation in a diffuser, but also altered the pressure distribution in a manner that allowed for improved pressure recovery. This improvement was realized by an increase in the pressure coefficient of between 30 and 38 percent, the larger increases occurring for those diffuser geometries most likely leading to stall (high aspect ratio). Additionally, it was discovered that the introduction of static ports into the riblet surface did not significantly alter the flowfield over that of a geometrically similar riblet surface.

14. SUBJECT TERMS	15. NUMBER OF PAGES
Riblets, pressure recovery, pressure coefficient, diffuser, flow separation	85
	16. PRICE CODE

17. SECURITY CLASSIFICATION OF REPORT	18. SECURITY CLASSIFICATION OF THIS PAGE	19. SECURITY CLASSIFICATION OF ABSTRACT	20. LIMITATION OF ABSTRACT
Unclassified	Unclassified	Unclassified	UL

GENERAL INSTRUCTIONS FOR COMPLETING SF 298

The Report Documentation Page (RDP) is used in announcing and cataloging reports. It is important that this information be consistent with the rest of the report, particularly the cover and title page. Instructions for filling in each block of the form follow. It is important to **stay within the lines to meet optical scanning requirements.**

Block 1. Agency Use Only (Leave Blank)

Block 2. Report Date. Full publication date including day, month, and year, if available (e.g. 1 Jan 88). Must cite at least the year.

Block 3. Type of Report and Dates Covered. State whether report is interim, final, etc. If applicable, enter inclusive report dates (e.g. 10 Jun 87 - 30 Jun 88).

Block 4. Title and Subtitle. A title is taken from the part of the report that provides the most meaningful and complete information. When a report is prepared in more than one volume, repeat the primary title, add volume number, and include subtitle for the specific volume. On classified documents enter the title classification in parentheses.

Block 5. Funding Numbers. To include contract and grant numbers; may include program element number(s), project number(s), task number(s), and work unit number(s). Use the following labels:

C	- Contract	**PR**	- Project
G	- Grant	**TA**	- Task
PE	- Program Element	**WU**	- Work Unit Accession No.

Block 6. Author(s). Name(s) of person(s) responsible for writing the report, performing the research, or credited with the content of the report. If editor or compiler, this should follow the name(s).

Block 7. Performing Organization Name(s) and Address(es). Self-explanatory.

Block 8. Performing Organization Report Number. Enter the unique alphanumeric report number(s) assigned by the organization performing the report.

Block 9. Sponsoring/Monitoring Agency Names(s) and Address(es). Self-explanatory.

Block 10. Sponsoring/Monitoring Agency. Report Number. (If known)

Block 11. Supplementary Notes. Enter information not included elsewhere such as: Prepared in cooperation with...; Trans. of ..., To be published in .... When a report is revised, include a statement whether the new report supersedes or supplements the older report.

Block 12a. Distribution/Availablity Statement. Denote public availability or limitation. Cite any availability to the public. Enter additional limitations or special markings in all capitals (e.g. NOFORN, REL, ITAR)

DOD	- See DoDD 5230.24, "Distribution Statements on Technical Documents."
DOE	- See authorities
NASA	- See Handbook NHB 2200.2.
NTIS	- Leave blank.

Block 12b. Distribution Code.

DOD	- DOD - Leave blank
DOE	- DOE - Enter DOE distribution categories from the Standard Distribution for Unclassified Scientific and Technical Reports
NASA	- NASA - Leave blank
NTIS	- NTIS - Leave blank.

Block 13. Abstract. Include a brief (Maximum 200 words) factual summary of the most significant information contained in the report.

Block 14. Subject Terms. Keywords or phrases identifying major subjects in the report.

Block 15. Number of Pages. Enter the total number of pages.

Block 16. Price Code. Enter appropriate price code (NTIS only).

Blocks 17. - 19. Security Classifications. Self-explanatory. Enter U.S. Security Classification in accordance with U.S. Security Regulations (i.e., UNCLASSIFIED). If form contains classified information, stamp classification on the top and bottom of the page.

Block 20. Limitation of Abstract. This block must be completed to assign a limitation to the abstract. Enter either UL (unlimited) or SAR (same as report). An entry in this block is necessary if the abstract is to be limited. If blank, the abstract is assumed to be unlimited.